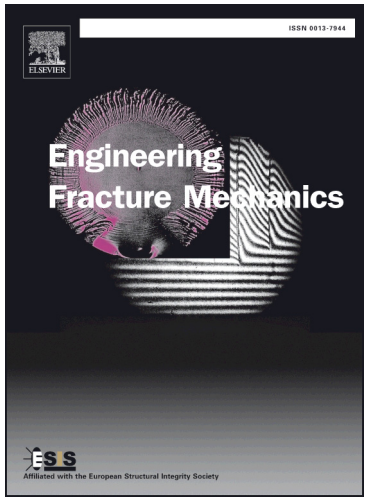

An adaptive stochastic multi-scale method for cohesive fracture modelling of quasi-brittle heterogeneous materials under uniaxial tension

R.M. Sencu, Z. Yang, Y.C. Wang

PII: S0013-7944(16)30058-3
DOI: http://dx.doi.org/10.1016/j.engfracmech.2016.02.040
Reference: EFM 5081

To appear in: *Engineering Fracture Mechanics*

Received Date: 27 September 2015
Revised Date: 17 February 2016
Accepted Date: 18 February 2016

Please cite this article as: Sencu, R.M., Yang, Z., Wang, Y.C., An adaptive stochastic multi-scale method for cohesive fracture modelling of quasi-brittle heterogeneous materials under uniaxial tension, *Engineering Fracture Mechanics* (2016), doi: http://dx.doi.org/10.1016/j.engfracmech.2016.02.040

An adaptive stochastic multi-scale method for cohesive fracture modelling of quasi-brittle heterogeneous materials under uniaxial tension

R. M. Sencu[1], Z. Yang[2*], Y. C. Wang[1]

[1] School of Mechanical, Aerospace and Civil Engineering, University of Manchester, M13 9PL, UK

[2] Faculty of Engineering, Computing and Environment, Coventry University, CV1 2JH, UK

Abstract

An adaptive stochastic multi-scale method is developed for cohesive fracture modelling of quasi-brittle heterogeneous materials under uniaxial tension. In this method, a macro-domain is first discretised into a number of non-overlapping meso-scale elements (MeEs) each of which containing detailed micro-scale finite element meshes. Potential discrete cracks in the MeEs are modelled by pre-inserted cohesive interface elements (CIEs). Nonlinear simulations are conducted for the MeEs to obtain the crack patterns under different boundary conditions. The macro-domain with the same number of overlapped, adaptively size-increasing MeEs are then simulated, until the potential cracks seamlessly cross the boundaries of adjacent MeEs. The resultant cracks, after being filtered by a new Bayesian inference algorithm to remove spurious cracks wherever necessary, are then integrated as CIEs into a final anisotropic macro-model for global mechanical responses. A two-dimensional example of carbon fibre reinforced polymers was modelled under two types of uniaxial tension boundaries. The developed method predicted crack patterns and load-displacement curves in excellent agreement with those from a full micro-scale simulation, but consuming considerably less computation time of the latter.

Keywords: *multi-scale stochastic fracture mechanics; scale coupling; cohesive crack model; overlapping elements; fibre reinforced plastics.*

1. INTRODUCTION

Due to the random distribution of multiple phases from nano-, micro-, meso- to macro-scales, multiphase quasi-brittle materials, such as concrete and fibre-reinforced polymers (FRP) have intrinsically stochastic, heterogeneous and nonlinear physical and mechanical properties across the multi-length scales. As the finer-scale properties directly determine the performance and reliability of structures and systems at coarser-scales, better understanding of these properties and their inter-scale relationships or scale-transferability by multi-scale computational modelling, has become a critical problem (de Borst, 2008; Kassner et al., 2005; Oden et al., 2003; Kanouté et al., 2009; Nguyen et al., 2012a). This is particularly true for fracture problems, as fracture always starts from micro-cracks at strain localization sites, which then propagate, widen and coalesce into meso-cracks and finally discrete macro-cracks. This phenomenon spans a few length scales, demanding a multi-scale modelling approach.

In general, there exist two categories of multi-scale modelling approaches (Belytschko, 2007): (1) concurrent ones, where multiple scales of computing are performed simultaneously; (2) hierarchical or sequential ones, where fine-scale problems are solved in sub-domains and the homogenised results are up-scaled separately in coarse-scale computing.

In modelling fracture problems, the concurrent approaches naturally discretise the regions with strain localisation by fine meshes and the other by coarse meshes to save computational cost. It is particularly useful for problems with a few cracks or weak interfaces known a priori, where the crack-tip and the interfacial regions are modelled in detail for accurate understanding of the fracture mechanism at fine scales (e.g., (Ghosh and Paquet, 2013; Ghosh et al., 2007; Canal et al., 2012; González and Llorca, 2006; Trias et al., 2006a; Trias et al., 2006b; Trias et al., 2006c; Li et al., 2013)). However, for problems with many distributed cracks or unknown cracks, very dense meshes may have to be used in the whole domain to simulate potential cracks, making the concurrent approaches computationally costly.

In the hierarchical approaches, a representative volume element (RVE) or unit cell, based on the classical homogenization theory (Hill, 1963; Hashin, 1965), is assumed to exist at medium scales. Once the existence and size of the RVE is determined by detailed numerical analyses in fine scales, the domain at coarse scales is assumed homogeneous and modelled by a number of RVEs. In doing so, a full analysis of the domain with fine-scale details is avoided. However, recent studies (Phu Nguyen et al., 2010; Gitman et al., 2008; Gitman et al., 2007) find that the RVE exists only in linear-elastic and hardening regimes; once softening occurs as in fracture and damage, the material loses the "representative" properties and the RVE cannot be found, because the material in softening shows localization leading to the loss of statistical homogeneity. If the RVE does not exist, special measures must be taken for multi-scale modelling to maintain the objectivity with respect to the size of the sample cells. Various multi-scale models have been recently developed to solve this dilemma, e.g., the coupled-volume multi-scale model (Gitman et al., 2008), the multi-scale aggregating discontinuities model (Belytschko et al., 2008; Loehnert and Belytschko, 2007), the multi-grid method (Miehe and Bayreuther, 2007; Kaczmarczyk et al., 2010), the homogenization-localization methods (Bosco et al., 2015; Coenen et al., 2012), the enhanced continuous-discontinuous model (Nguyen et al., 2012b; Nguyen et al., 2011), the reduced integration order model (Fish, 2011; Fish

and Shek, 1999), the two-scale homogenization model (Greco et al., 2013; Cusatis and Cedolin, 2007; Desmorat and Lemaitre, 2001), the multi-fractal approach (Carpinteri et al., 2002; Carpinteri and Chiaia, 1997; Xu et al., 2013), and the variational and localized Lagrange multiplier method (Hautefeuille et al., 2012; Markovic and Ibrahimbegovic, 2004).

It can be noted that most of the existing multi-scale models, either concurrent or hierarchical, have tackled fracture problems with single, a few cracks or pre-defined bi-material interfaces. The fine-scale multiphase structures are mostly assumed and the numerical results are difficult to be accurately validated. The latest advances in high-resolution image-based models (Dirrenberger et al., 2014; Ren et al., 2015; Huang et al., 2015) appear very promising for direct validation of the numerical models but they are so far not used in multi-scale modelling and validation. In addition, multi-scale models considering the effects and inter-scale transfer of stochastic information are still largely limited to the prediction of homogenised elastic properties (Xu and Graham-Brady, 2005; Xu and Chen, 2009) rather than complicated fracture evolution. 3D multi-scale modelling of fracture in composite materials has rarely been reported, probably due to the very large number of degrees of freedom in the fine-scale models that are beyond the power of conventional computers. Therefore, much research is still needed to develop more robust multi-scale methods for complicated fracture modelling, as also pointed out by a relatively recent report of USA National Committee on Theoretical and Applied Mechanics (Belytschko, 2007).

As an effort towards overcoming the above deficiencies, a new efficient multi-scale method is developed in this study for modelling complicated fracture behaviour in heterogeneous quasi-brittle materials. In this method, a macro-domain is first discretised into a number of meso-scale elements (MeEs) with detailed micro-scale finite element meshes generated from images obtained by a microscope. The initiation and propagation of multiple cracks is modelled discretely by pre-inserted cohesive interface elements (CIEs) with tension and shear softening laws (Yang et al., 2009; Su et al., 2010). The number and the size of the MeEs required are determined by a size effect study with respective to crack paths and strength. A nonlinear simulation is then conducted separately for each MeE in parallel to obtain the crack patterns under two types of uniaxial tensile boundary conditions. The same number of overlapped, adaptively size-increasing MeEs are then simulated, until the cracks seamlessly cross the boundaries of adjacent MeEs. This can be achieved because the shared microstructures within the neighbouring overlapped elements minimise the potential crack bias and the boundary deformation incompatibility across boundaries. After being filtered by the Bayesian inference algorithm to remove spurious cracks wherever necessary, the resultant cracks are integrated as CIEs (with softening laws mapped from the adaptive meso-scale study) into a final anisotropic macro-model to compute the global responses. The crack patterns and load-displacement curves computed from the developed method are compared with those from a full micro-scale simulation as a means of numerical validation.

It should be noted that the overlapping strategy used herein is similar to the oversampling strategy used in the so-called generalised multi-scale finite element method (GMsFEM) for flow problems in heterogeneous porous media (Hou and Wu, 1997; Chen et al., 2003; Aarnes et al., 2006; Efendiev et al., 2004; Efendiev et al., 2014; Calo et al., 2014). In the GMsFEM, the scale-coupling is realised using multi-scale basis functions containing the deformation information of fine-scale elements. The oversampling strategy uses larger regions than the fine-scale elements to construct more accurate

local basis functions, making the GMsFEM converge faster with fewer degrees of freedom. Although the GMsFEM with oversampling has recently been applied to linear elastic stress analyses (Chung et al., 2014) and seismic wave propagation (Gao et al., 2014), its extension to complicated nonlinear fracture problems is not yet reported. Such an extension is very challenging due to the strain localisation and associated nonlinear material softening, which may presumably make it impossible to form the rigorous analytical derivation of the GMsFEM to ensure deformation compatibility between the fine-scale elements for general external boundary conditions.

As the first attempt to use the overlapping strategy for multi-scale cohesive fracture modelling in quasi-brittle materials, this study will investigate problems with randomly and evenly distributed inclusions and predominantly mode-I fracture, so that all the meso-scale elements are assumed under uniaxial tension and can be modelled independently. The overlapping grids with common areas are used to enhance the deformation compatibility. The scale transfer is realised by the energy conservation principle through mapping the traction-displacement softening curves in CIEs from the MeEs to the MaEs. The effects of inclusion-matrix interfacial fracture properties and two types of boundary conditions on the crack path and strength are also investigated. A two-dimensional example of FRP plates is modelled as a case study.

2. METHODOLOGY

2.1. Framework

Figure 1 shows the framework of the developed method with the key modules highlighted. It starts with acquiring a high-resolution image of the global domain by micro-tests using advanced techniques such as high-resolution cameras, microscopes and X-ray Computer Tomography (XCT). The image is then processed and segmented into different phases. If the crack paths and load-carrying capacities are not available from the micro-tests, a full micro-scale FE modelling of the global domain is carried out to validate the multi-scale modelling. In this case, the global-domain image is first transformed into FE meshes of solid elements. Cohesive interface elements with softening traction-displacement constitutive laws in normal and shear directions are then inserted into the matrix mesh and between the matrix-inclusion interfaces, to model potential cracks. This method has proved to be very effective in modelling complicated 2D and 3D meso-scale fracture processes in concrete, using the random field theories (Yang et al., 2009; Su et al., 2010), direct generation and packing of aggregates (Wang et al., 2015; Caballero et al., 2008), and XCT image-based models (Ren et al., 2015). Other approaches, such as dynamically inserting CIEs only when a certain criterion is reached (Yu et al., 2008; Ruiz et al., 2001; López et al., 2007), can also be used to improve the computational efficiency.

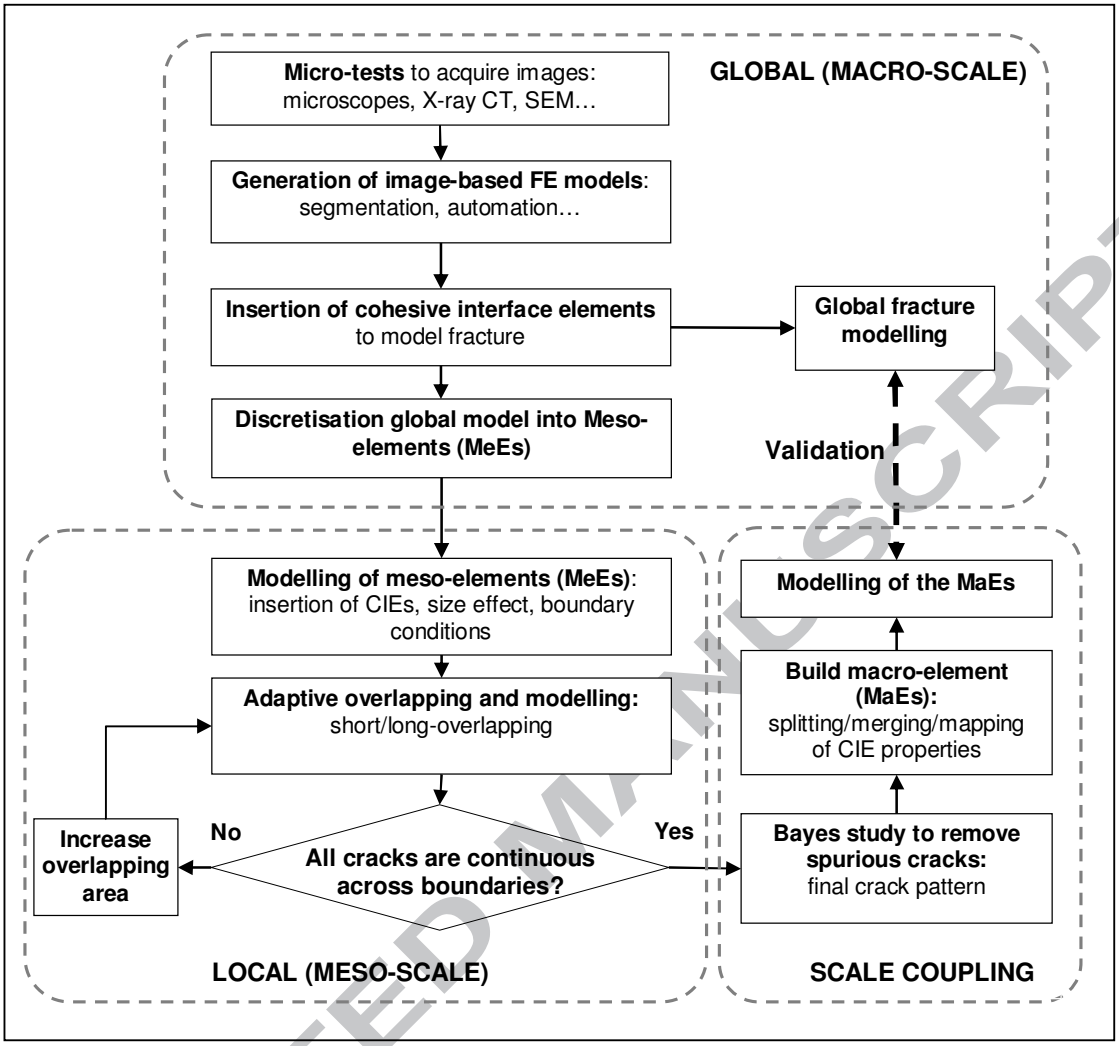

Figure 1: A two-scale coupling scheme for stochastic fracture mechanics.

The global domain is then divided into a grid with a number of non-overlapped rectangular meso-elements (MeEs), illustrated in Figure 3(a) as an example. For each MeE, its micro-structure is meshed with CIEs inserted and a nonlinear FE analyse is conducted under the same boundary condition. Size effect studies on the strength are carried out to determine a proper number and size of the MeEs. Two boundary conditions as illustrated on the first row in Figure 2, noted as B1 and B2 are necessary for the MeEs and scale transfer. The B1 is the uniaxial tensile condition and B2 is the shear condition necessary for the nonlinear integration of tractions for the global CIEs. At the global scale, two types of external uniaxial boundary conditions G1 and G2 are modelled, as illustrated in Figure 2(c) and 2(d), respectively. The popular G1 condition tends to result in the pure mode-I fracture mode, while the G2 allows core rotations and may lead to two main cracks. The G2 condition has also been increasingly used (Park and Paulino, 2012; Wang et al., 2015; Ren et al., 2015). In this paper, this was not implemented as a boundary condition for the scale transfer.

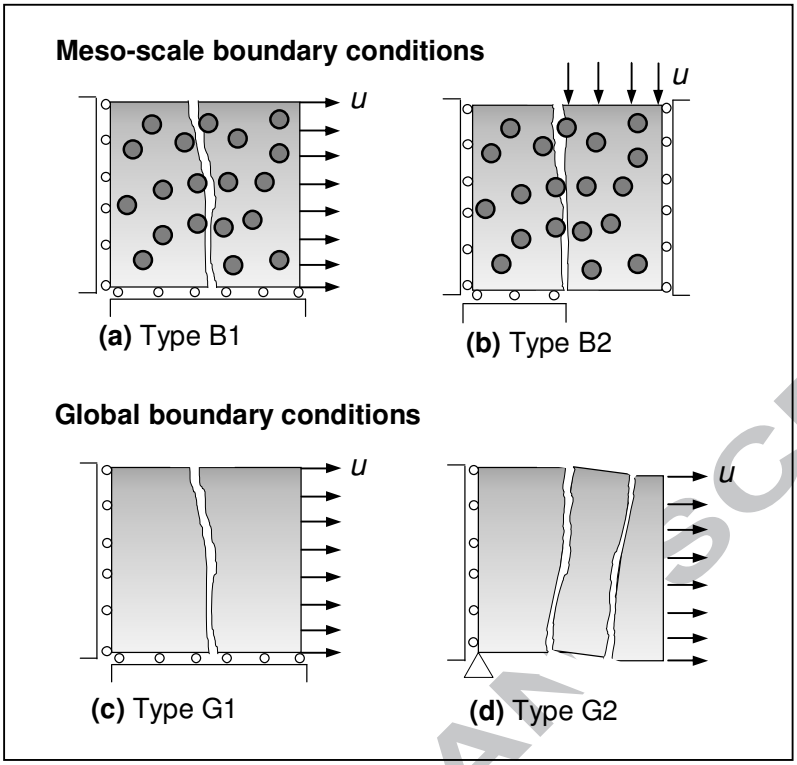

Figure 2: Boundary conditions for meso-scale modelling and for the global multi-scale models.

Figure 3(b) shows the crack paths from 16 independent nonlinear simulations of MeEs under the B1-X condition (X means horizontal and Y vertical direction).

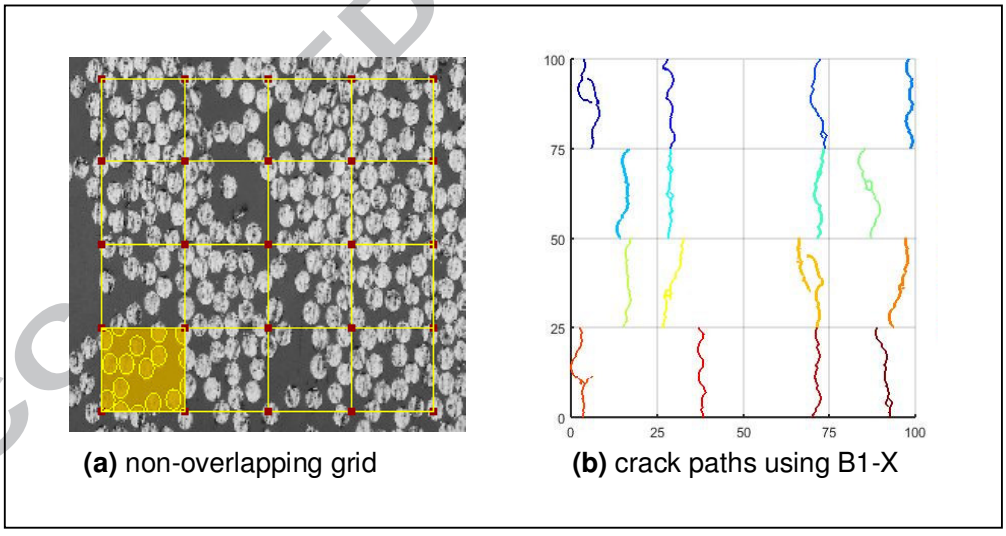

Figure 3: (a) A global domain discretised into 16 non-overlapped MeEs and (b) the modelled crack paths for each MeEs independently under B1-X boundary condition.

From Figure 3(b) it can be seen that not all the cracks across the MeEs' boundaries are continuous, indicating that deformation compatibility does not hold. This usually occurs when the non-overlapping grid is used. To improve the situation, an overlapping grid (Figure 4(a)) with the same

number but larger size MeEs is then designed. All the MeEs are again modelled independently. The resulting crack paths are shown in Figure 4(b). It can be seen that most of the crack paths now cross the MeEs' boundaries continuously, indicating improvement of the overlapping grid over the non-overlapping grid (Figure 3(b)). Subsequent overlapping grids with larger MeEs can be further designed and modelled if necessary. Figure 4(c) shows the final crack paths which nearly seamlessly cross all the MeEs' boundaries. This algorithm of using adaptively size-increasing overlapping grids works because the larger the overlapping regions become, the better deformation compatible support is provided.

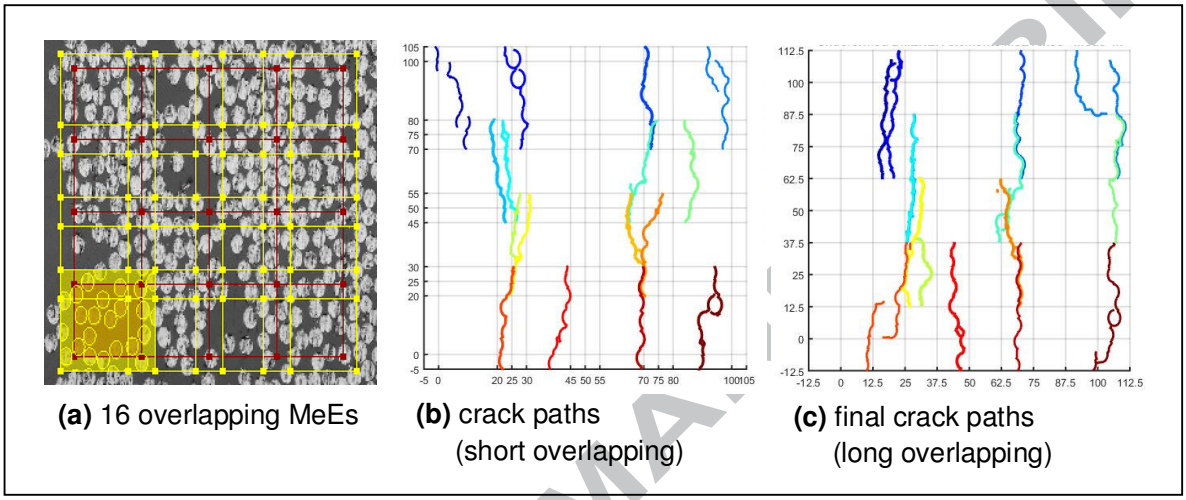

Figure 4: Overlapping MeEs and crack paths under B1-X boundary.

2.2. Bayesian inference model for overlapping MeEs with non-matching crack paths

Because the MeEs are separately modelled and the deformation compatibility cannot be rigorously ensured, some non-physically overlapped crack paths may be predicted, as seen in Fig. 4. To improve this situation, the Bayesian inference model is applied to filter the crack paths and preserve the most critical cracks only for subsequent scale transfer.

The well-known Bayesian inference method is

$$P(C|E)=\frac{P(E|C)}{\sum_m P(E|C_m)P(C_m)}\cdot P(C) \qquad \text{Equation 1}$$

Assume that the fracture process generates independent crack events E under similar boundary conditions but with unknown probability distribution. Equation 1 updates the degree of matching of a kernel crack path with m number of neighbouring cracks C_m (see Fig. 5). For each non-boundary kernel MeE, for example, there are 8 adjacent MeE each with a crack path so m=1~8. Assume that the denominator in Equation 1 can be represented by equally distributed probabilities $P(C_m)$ with known values for all adjacent half-overlapping and quarterly-overlapping MeEs with $\sum_{m=8} P(C_m)=1$. The probability $P(E|C_m)$ (m=1~8) remain fixed over the cluster C_m. It can be seen that Equation 1 updates the prior probability $P(E|C)$ to posterior probability $P(C|E)$ given a target probability $P(C)$. The $P(E|C)$ can be then used as a threshold to filter the cracks.

In the present paper the probabilities $P(E|C)$ and $P(C)$ are calculated as a surface/path integral, which can be reduced to a discrete number of key points at known locations as

$$P(C) = \int_C f(H_k) dH_k \qquad \text{Equation 2}$$

where the crack path is parameterised by a function $f(H_k)$ where H_k are key points on the crack path C. Alternatively Equation 2 can be calculated using the pixels forming the crack path in the images.

Fig. 5(a) illustrates two types of grid-free cracks: overlapping domain cracks and non-overlapping domain cracks when short overlapping is used. If the overlapping length is equal to or larger than half the MeE grid distance, the grid-free non-overlapping cracks merge into grid-free overlapping cracks. This becomes valid for all the non-boundary MeE due to full overlapping length. If the overlapping length exceeds half of the MeE grid distance, double overlapping regions appear. Due to the complexity in multiscale transfer, this study only deals with single overlapping grids of full-length, which bounds the long overlapping criteria to half the length of MeE size.

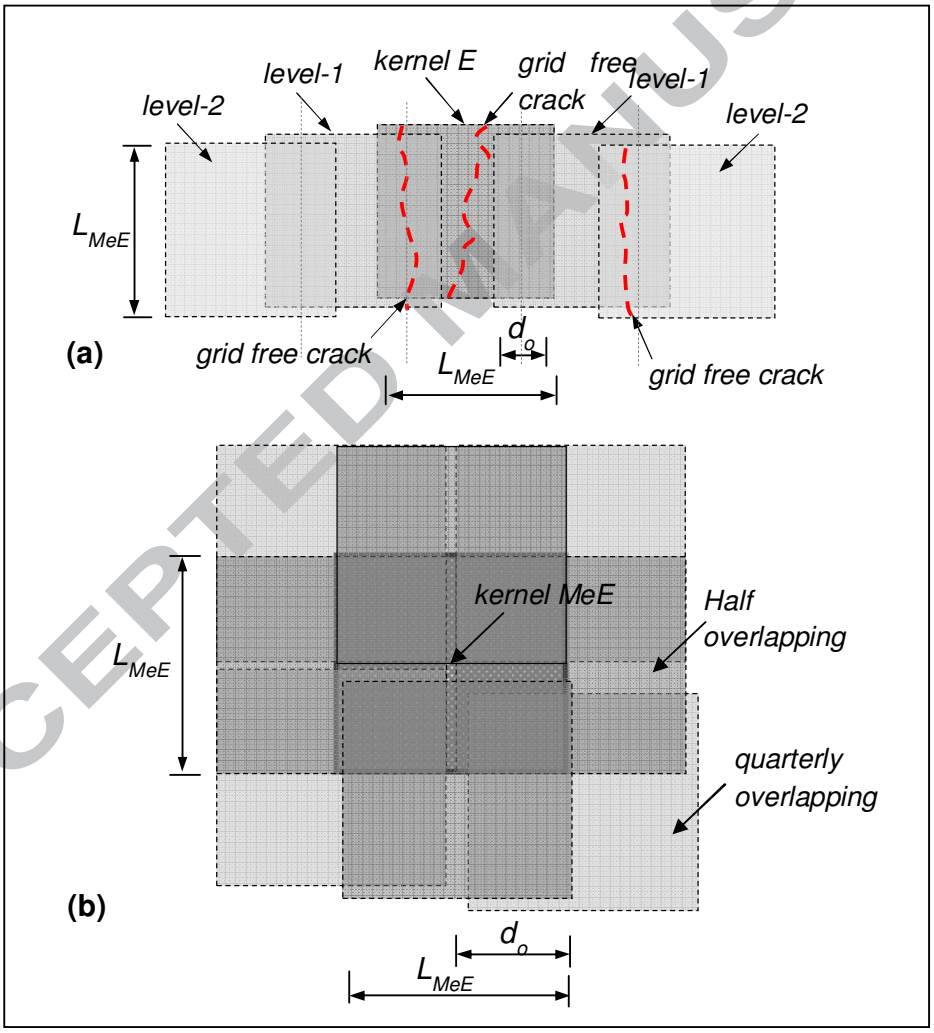

Figure 5: Illustration of crack sampling cases for the overlapping windows concept used with Bayesian criterion in Equation 1. The dark-shaded elements represent four half overlapping elements and soft-shaded elements represent four quarterly overlapping elements.

To quantify the matching degree with less computational effort, only two key points are initially used, i.e, the points of a crack path intersecting the non-overlapping grid. These points are suitable for any overlapping MeE sizes but may be unsuitable when multiple boundary conditions are simultaneously used. Therefore, the general case is implemented using matrices based on pixel metrics. Fig. 6 shows the implemented procedure and the results on an MeE using the half overlapping criteria.

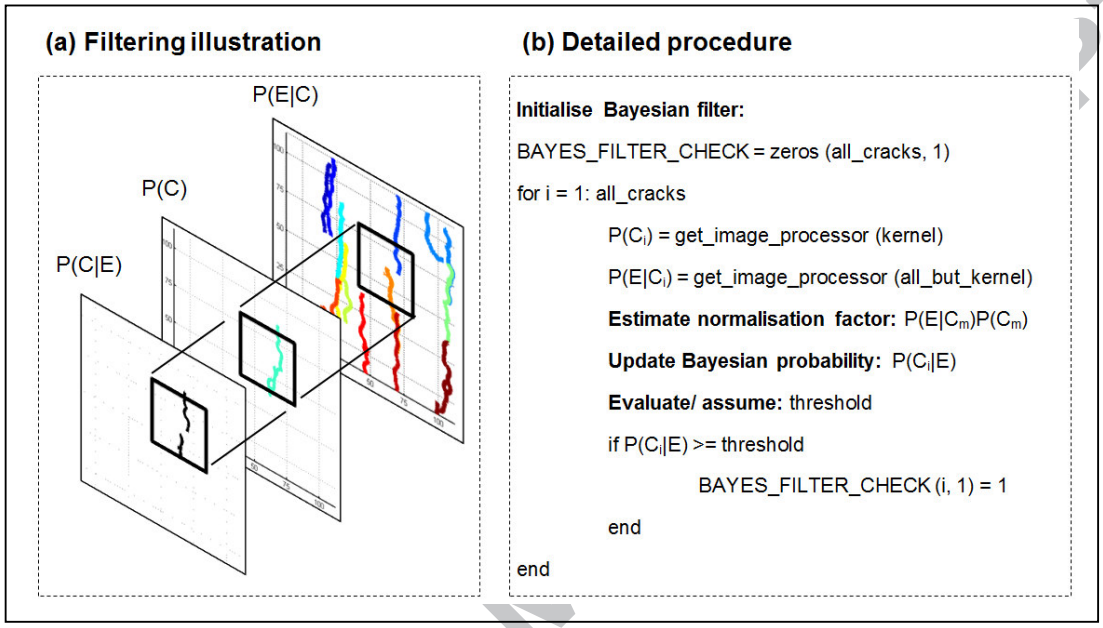

Figure 6: Bayesian filtering procedure and threshold probability on a typical non-boundary MeE

Fig. 7 shows the crack paths after using the Bayesian filtering method for two cases using the short and long overlapping grids.

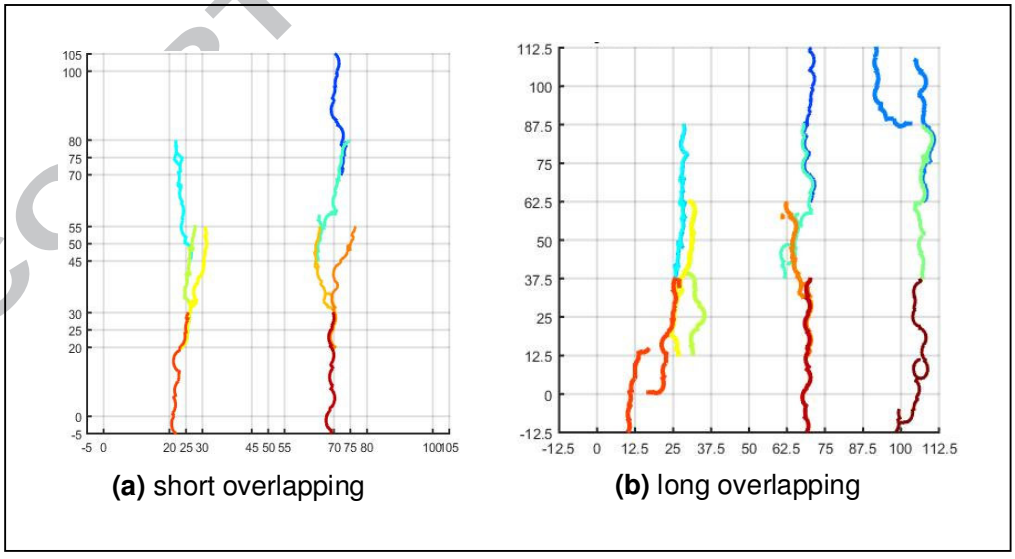

Figure 7: Filtered overlapping MeE crack path data after using the Bayesian inference model corresponding to Figure 4(b) & (c).

2.3. Construction of macro-scale elements (MaEs)

In general, short and long overlapping can be used as illustrated in Figure 8. This depends on the size establishment as for the MeE overlapping grid and are limited to single overlapping regions in this paper. This means that the size of an overlapping MeE cannot be larger than twice the MeE non-overlapping grid size (see Figure 3 (a) & Figure 4 (a)). In this paper, it is found that for defective materials, the short to long overlapping method may be used. For less defective materials, non-overlapping as for elastic studies or short overlapping discretisation in fracture mechanics may be used.

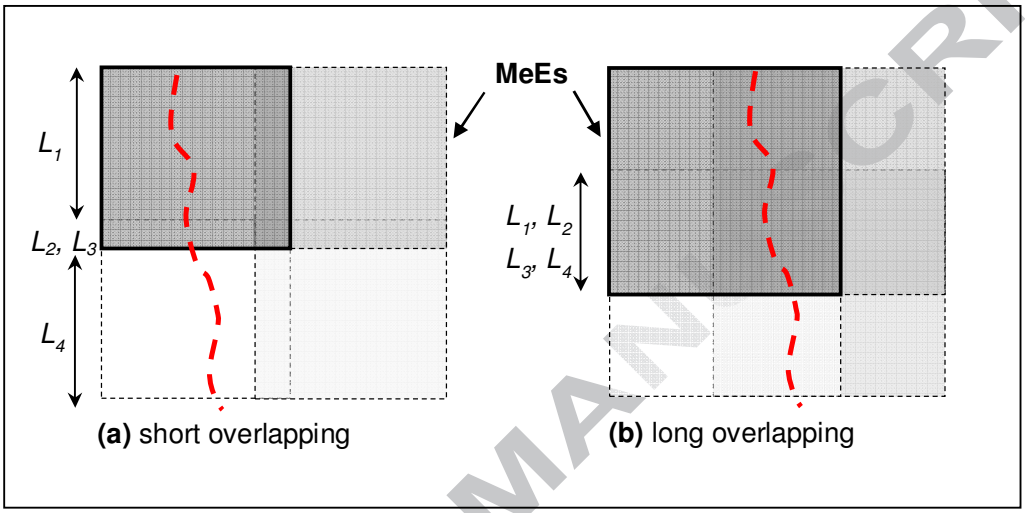

Figure 8: Illustration of (a) short to (b) long overlapping criteria. The colour intensities represent distinct MeE windows that are overlapped. The average fracture properties from corresponding crack path lengths denoted with L_i, where i is the corresponding overlapped crack path, are integrated piecewisely and transferred to the macro-scale by inserting cohesive elements.

After the optimised crack paths are found, macro-elements (MaEs) are constructed. The final meso-scale crack paths and non-overlapping grids are naturally used as guidelines to discretise the domain into a macro-mesh with a number of MaEs. In the macro-mesh, the crack paths are also modelled by CIEs whose softening constitutive laws are piecewisely mapped from the meso-CIEs, so that energy conservation is ensured in the scale transfer (see Figure 9).

The macro-scale mesh discretisation includes the intersection nodes, the assembly of the MaE model and the insertion of macro-cohesive interface elements. Figure 9 sketches two possible mesh models. The crack paths are identified based on the scalar degradation parameter d and the energy dissipation rate per unit volume of damage. In the case of short overlapping MeEs, the MaE nodes are at the intersections of the crack paths that cross cut the non-overlapping grids. The example illustrated in Figure 9 uses the B1-X boundary conditions. Two operations are used in the construction of the macro-meshes: merging and splitting (see Figure 9 (a) & (b)). These operations are generally used to reduce the integration order of the macro-model. However, they also become necessary when the crack path is very close or intersecting the non-overlapping grid. Their implications on the energy mapping rules are discussed in next section.

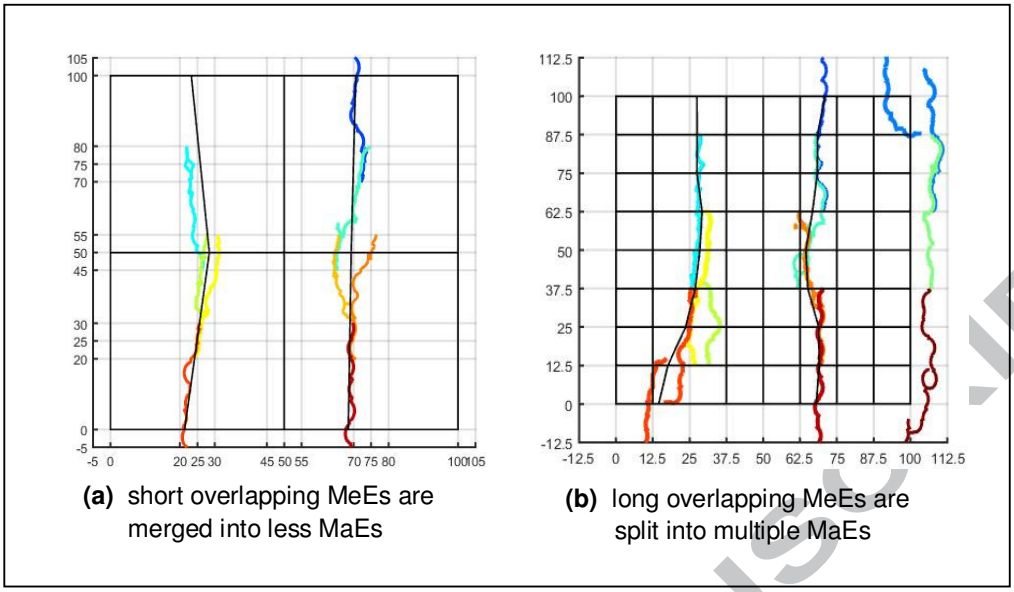

Figure 9: Illustration of two possible macro-scale meshes. The crack paths are used as boundary constraints during the MaE mesh generation. The cracks are also represented by cohesive interface elements (CIE) in the global model.

In fact, many other mesh models can be created at global length scale once the most critical crack paths available from the detailed simulations. For example, it is possible to build reduced integration meshes, either by using triangular or non-structured quads or by keeping details of the heterogeneous meso-scale mesh with coarser macro-elements and only inserting cohesive elements or enrichment nodes where necessary. However, there are some sources of uncertainty associated with the above strategy, for example:

- the centreline of the deformed cohesive crack MaEs may not be the same as the initial zero-thickness crack path which is used to build the MaE elements; this is due to the reversing of damage process for crack identification paths which were obtained using prescribed boundary conditions based on the stochastic element cluster assumption.
- the superposed straight edges of MaE elements in reduced order strategies may not be in line with the true integration crack paths which have a certain tortuosity; however, it is a reasonable assumption when using invariant crack paths to MeE boundary effects. This strategy can be used to reduce the global model size considerably.
- using more complicated mixed-mode boundary conditions (BCs) and highly non-homogeneous distributions of defects, two dominant crack failure modes can appear which may be tackled with a rotational centre. This imposes geometrical non-linearity in the macro-cohesive model which was not tested in this paper.

2.4. Energy mapping rules

After the macro-mesh is constructed, the traction-displacement softening curves of macro-CIEs need to be mapped from the meso-CIEs at the same position to ensure energy conservation.

The conversion of stress displacement curves in fracture energy is done according to the assumption in (Hillerborg et al., 1976) which defines the fracture energy required to open a unit area of crack by:

$$G_f = \int_{u_0}^{u_f} \sigma_{f,u} du \qquad \text{Equation 3}$$
$$\sigma_{f,u} = \sigma(u)$$

where σ_f and u_0 are the ultimate strength and displacement at the onset of fracture.

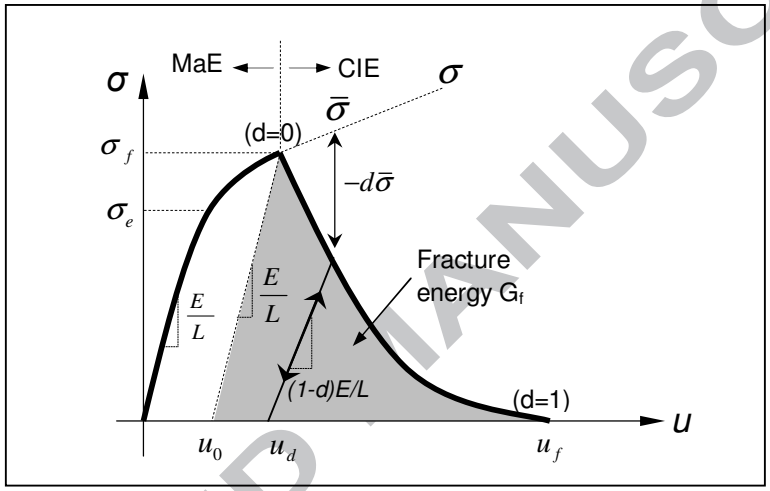

Figure 10: Illustration of the stress-displacement curve for the macro-scale bulk material properties. $\bar{\sigma}$ is the stress due to no damage, d is the scalar degradation variable and L is the characteristic length (Simulia/Abaqus).

For accurate integration across the scale transfer, L in Figure 8 can be represented by the actual crack length. This is feasible when appropriate scale discretisation and mesh order reduction strategy is considered. To prove the suitability of the new multi-scale concept, ABAQUS/Explicit is used in Section 3. In general, the estimated fracture energy from the collection of detailed MeE integration domains is consumed at macro-scale by the opening of macro cohesive elements. The method can be implemented by using both non-overlapping and overlapping adaptive strategy as discussed above. However, because the strategy uses fixed or enlarged computational areas but multiple parallel windows, this particular concept can be used to capture localized fracture behaviour with lower single simulation computational effort compared with large full-size detailed models. Two other advantages of the overlapping approach in this paper are: the capability of coupling weak to relatively strong interface models and its fully anisotropic formulation for analyses of complicated materials. This means that larger MeE windows can be adaptively employed for modelling materials with various degrees of flaws and fully anisotropic properties at any length scale. A case study for CFRP materials is presented in Section 3.

Different energy mapping rules are derived for merging and splitting operation respectively, considering both short and long overlapping.

2.4.1. Merging & splitting approach (MSA)

MSA is an edge oriented multi-scale cohesive crack model. The neighbour cluster of stochastic MeEs is either merged into larger size MaEs or split into several smaller size MaEs. The fracture energy dissipated is derived accordingly for the general cases based on average weighting factors of the overlapping regions as given in Equation 4 & Equation 5 for short and long overlapping respectively. Therefore, it should be noted that before using these two mapping rules, the existence of L_i factors contributing towards the macro-CIE should be first checked (see Figure 8).

$$G_{f,short} = \int_{u_0}^{u_f} \sigma_{f,L1} du + \frac{1}{2}\left(\int_{u_0}^{u_f} \sigma_{f,L2} du + \int_{u_0}^{u_f} \sigma_{f,L3} du\right) + \int_{u_0}^{u_f} \sigma_{f,L4} du \quad \text{Equation 4}$$

$$G_{f,long} = \frac{1}{4}\left(\int_{u_0}^{u_f} \sigma_{f,L1} du + \int_{u_0}^{u_f} \sigma_{f,L2} du + \int_{u_0}^{u_f} \sigma_{f,L3} du + \int_{u_0}^{u_f} \sigma_{f,L4} du\right) \quad \text{Equation 5}$$

The crack evolution at macro-scale can be also defined by means of a scalar degradation variable d which ranges between 0 and 1 (see explanation in Figure 10). The linear formulation of d can be expressed as:

$$d = \frac{u}{u_f} \quad \text{Equation 6}$$

Combining the Equation 4 & Equation 5 with Equation 6, the linear degradation variables become:

$$d_{short} = \frac{1}{3}\left(\frac{2G_{f,L_1}}{u_{f,L_1}\sigma_{f,L_1}} + \frac{G_{f,L_2}}{u_{f,L_2}\sigma_{f,L_2}} + \frac{G_{f,L_3}}{u_{f,L_3}\sigma_{f,L_3}} + \frac{2G_{f,L_4}}{u_{f,L_4}\sigma_{f,L_4}}\right) \quad \text{Equation 7}$$

$$d_{long} = \frac{1}{4}\left(\frac{2G_{f,L_1}}{u_{f,L_1}\sigma_{f,L_1}} + \frac{2G_{f,L_2}}{u_{f,L_2}\sigma_{f,L_2}} + \frac{2G_{f,L_3}}{u_{f,L_3}\sigma_{f,L_3}} + \frac{2G_{f,L_4}}{u_{f,L_4}\sigma_{f,L_4}}\right) \quad \text{Equation 8}$$

The degradation rates d can be also expressed exponentially. To ensure that the total energy dissipation on softening equals the total fracture energy G_f, the following expressions are derived:

$$d_{short} = 1/3 d_1 + 1/6(d_2 + d_3) + 1/3 d_4 \quad \text{Equation 9}$$

$$d_{long} = 1/4(d_1 + d_2 + d_3 + d_4) \quad \text{Equation 10}$$

where d_i are the individual contributions of MeEs to the degradation of the macro-cohesive element as illustrated in Figure 8 and given by:

$$d_i = 1 - \exp\left(-\int_{u_0}^{u_f} \sigma_{f,u,Li} du \Big/ G_{f,Li}\right) \quad \text{Equation 11}$$

This ensures that the fracture energy is gradually consumed during each displacement increment u_{Li}.

2.4.2. Crack path decomposition approach (CDA)

The CDA is an explicit meta-model, in the sense that cohesive elements are inserted only where necessary, while the homogenized continuum elements MaEs are integrated correspondingly so as to preserve the individual phases or composite elasticity. The material properties of cohesive elements for the overlapped mesh can be avoided if similar crack paths are repeating. Therefore, the general energy mapping rule involving non-overlapping single cracks or single-split cracks that overlap such as in Figure 9 (b) reduces to:

$$G_{f,L_i} = \int_{u_0}^{u_f} \sigma_{f,u,Li} du \qquad \text{Equation 12}$$

where the linear degradation variables are:

$$d_i = \frac{2G_{f,L_i}}{u_{f,L_i}\sigma_{f,u,L_i}} \qquad \text{Equation 13}$$

and the exponential degradation variables are:

$$d_i = 1 - \exp\left(-\int_{u_0}^{u_f} \sigma_{f,u,Li} du \Big/ G_{f,Li}\right) \qquad \text{Equation 14}$$

in which *i* corresponds to the crack site which is replaced by a 4-noded cohesive element. L refers to the actual crack length which is replaced by macro-scale edges. Alternatively, an exact stress strain evolution can be used giving tabular inputs (Simulia/Abaqus).

2.5. Computer implementation and procedure

The above methodology is implemented in a number of computer programs which are integrated in a batch file for automatic simulations. The meshing and the extraction of traction-displacement curves of CIEs are done by Python scripts. Pre-inserting CIEs, the construction of MaEs and energy mapping are implemented in MATLAB codes.

The MeE overlapping series were computed on parallel CPUs. The CPU time on a desktop PC i7 – 2600 @3.40GHz with 8 cores was about 5 to 6 hours per simulation, while when using 48 cores per simulation on the CSF facility at University of Manchester, the average time was 45 min. The large validation models MeE size 100μm were also simulated using 48 cores and lasted about 14 hours each.

3. CASE STUDY

This section presents the results of a case study applying the proposed multi-scale method to a three phase material (fibre, matrix and interface) made of carbon fibre reinforced polymer (CFRP).

3.1. Geometrical surveying of a CFRP ply

A geometrical survey was carried out first within the thickness of a ply to investigate the volume fraction variations (see Figure 11). The searching approach is similar to the one originally used for aluminum alloys (Graham and Yang, 2002) .

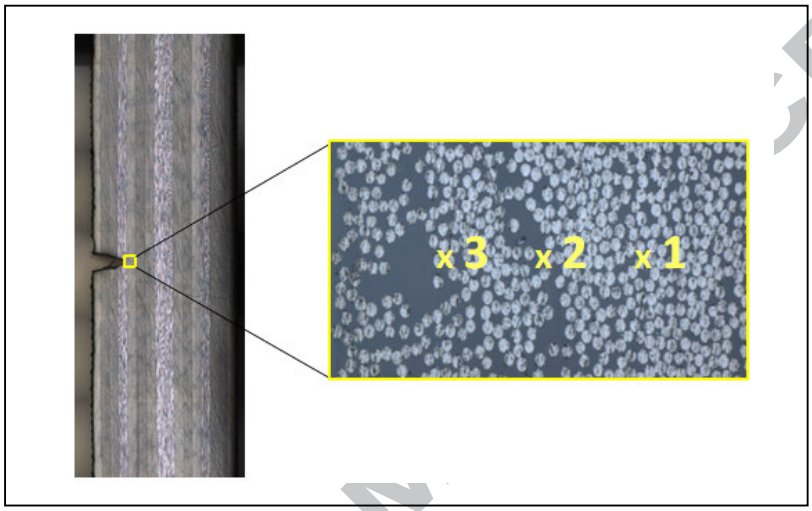

Figure 11: $+45^0$ ply in front of a notch tip (the numbers indicating positions of the centres of the imaging windows).

Figure 11 shows a micrograph extracted from a multi-layered CFRP beam with a V-notch. The images were acquired by image stitching from a laser confocal microscope. The micrograph covered the full thickness of a single layer of about 220µm. For this particular example, the fibres were elliptical shape of approximately 5µm of the shorter diameter because the ply ran at an inclined angle of +45 degrees. Three concentric square windows of different sizes were used to acquire the geometrical data. Figure 12 shows the typical acquisition windows at the mid position in Figure 11. Figure 13 summarises the surveying results.

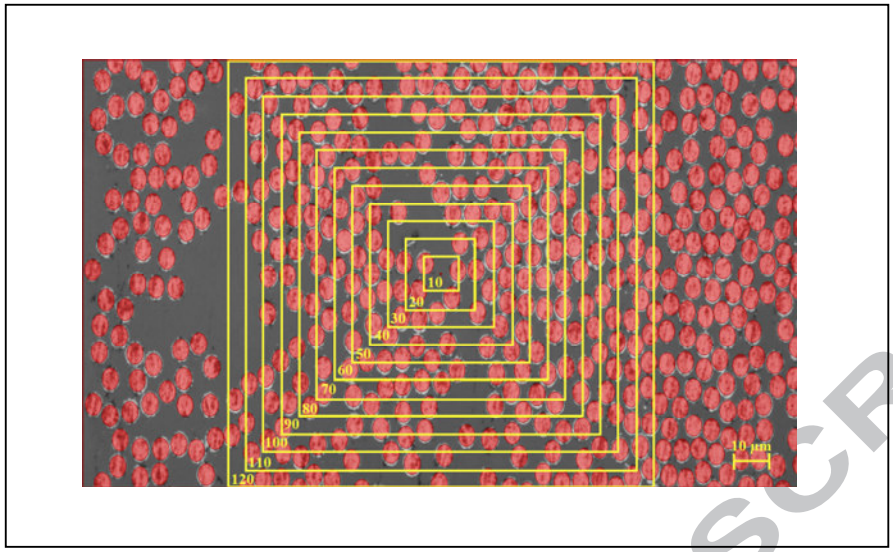

Figure 12: Surveying window sizes at position 2 in Figure 11.

Figure 13 also shows that within the ply thickness, the selection of the MeE window is morphologically important. The volume fraction statistics were found to be both position and size dependent. Apparently, the volume fractions converged when the window size was approximately 50µm^2, and the variation was more evident for small window sizes (10, 20 and 30µm^2) than larger sizes.

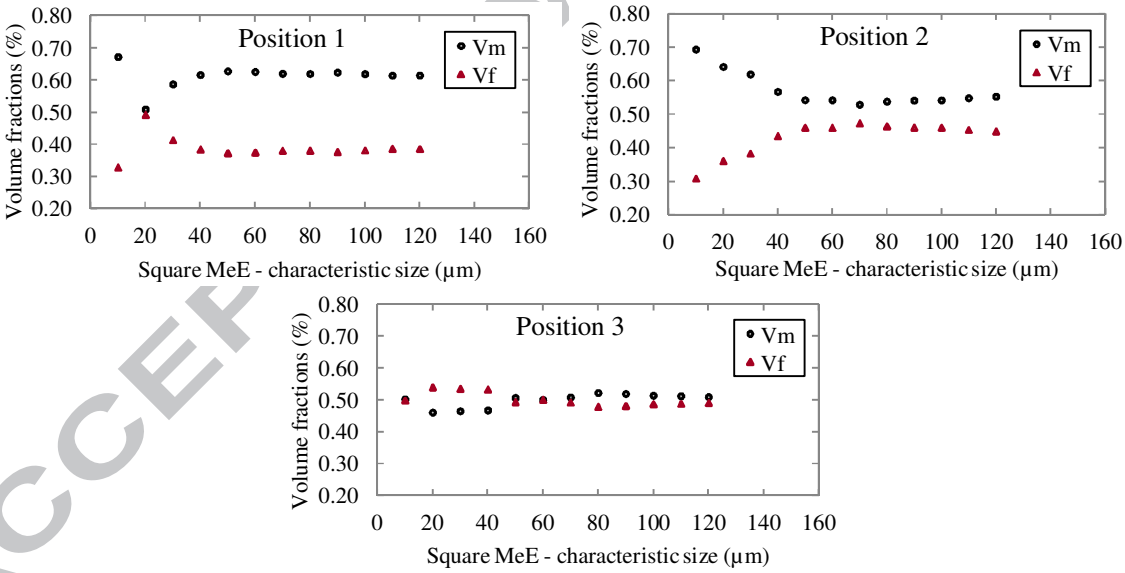

Figure 13: Variations of volume fractions of fibre (V_f) and matrix (V_m) with increasing MeE window size at different imaging positions for a carbon/epoxy ply +45°.

3.2. Material properties

Table 1 gives the main material parameters and the volume fractions used in the simulations. For simplification, it was assumed that the shear strength and fracture energy of each individual phase were equal to their normal ones respectively (Cid Alfaro et al., 2010; Vaughan and McCarthy, 2011; González and Llorca, 2007; Yang et al., 2009). Four types of fibre-matrix interfaces with different strength and fracture energy, namely, poor, weak, strong and perfect, were modelled here.

Table 1: Material properties and main modelling parameters.

	Carbon fibre	Epoxy resin	Interface
Elastic modulus E (GPa)	85	3.35	3.35
Poisson's ratio ν	0.22	0.35	0.35
Traction strength $t_n=t_s$ (MPa)	200	50	15 (poor), 25 (weak), 40 (strong), 50 (perfect)
Fracture energy $G_{fn}=G_{fs}$ (N/mm)	200E-03	50E-03	15E-03 (poor), 25E-03 (weak), 40E-03 (strong), 50E-03 (perfect)
Volume fraction (%)	30-60	70-40	-
Density (kg/m^3)		1500	

Table 2: Image based MeE simulations with modelling parameters.

Reference	Changing Parameters			Number of simulations per series
	Interface		Boundary conditions	
	$t_n=t_s$ (MPa)	$G_{fn}=G_{fs}$ (N/mm)		
MeE_10_100_W	25	25E-03	G1-X, G1-Y, G2-X, G2-Y	40
MeE_10_100_S	40	40E-03	G1-X, G1-Y, G2-X, G2-Y	40
MeE_16x25_P	15	15E-03	B1-X, B1-Y, B2-X, B2-Y	64
MeE_16x25_W	25	25E-03	B1-X, B1-Y, B2-X, B2-Y	64
MeE_16x25_S	40	40E-03	B1-X, B1-Y, B2-X, B2-Y	64
MeE_16x25_I	50	50E-03	B1-X, B1-Y, B2-X, B2-Y	64
MeE_16x35_W	25	25E-03	B1-X, B1-Y, B2-X, B2-Y	64
MeE_16x35_S	40	40E-03	B1-X, B1-Y, B2-X, B2-Y	64
MeE_16x50_W	25	25E-03	B1-X, B1-Y, B2-X, B2-Y	64
MeE_16x50_S	40	40E-03	B1-X, B1-Y, B2-X, B2-Y	64

Note: The first number of all series is the number of MeE windows. The second number in the MeE_10_100 series is the largest computed window in increments of size 10µm. The second number in the MeE_16x series is the overlapping grid size based on a non-overlapping grid base of size of 25µm.

3.3. Finite element modelling

The heterogeneous discretisation was performed using an in-house MATLAB code based on the pre-inserting cohesive element method in (Yang et al., 2009). At meso-scale, the finite element meshes consisted of triangular CPS3 solid elements and 4-noded cohesive interface elements COH2D4 in ABAQUS with linear traction-separation laws. The explicit dynamic solver with displacement control was used with adequate loading time for quasi-static loading condition.
Table 2 summaries the image-based simulations carried out with the boundary conditions and interface properties. All the other material properties used are shown in Table 1.

3.4. Validation of meso-scale modelling

Validation of the meso-scale modelling was conducted by comparison with results in (Cid Alfaro et al., 2010). An artificially created meso-scale window of S-glass fibre (30%) and epoxy resin was modelled. A good agreement was found in terms of stress contour plots and crack propagation patterns. Figure 14 shows the comparable fracture behaviour. The cracks are represented by the cohesive interface elements with damage index $D \geq 0.9$.

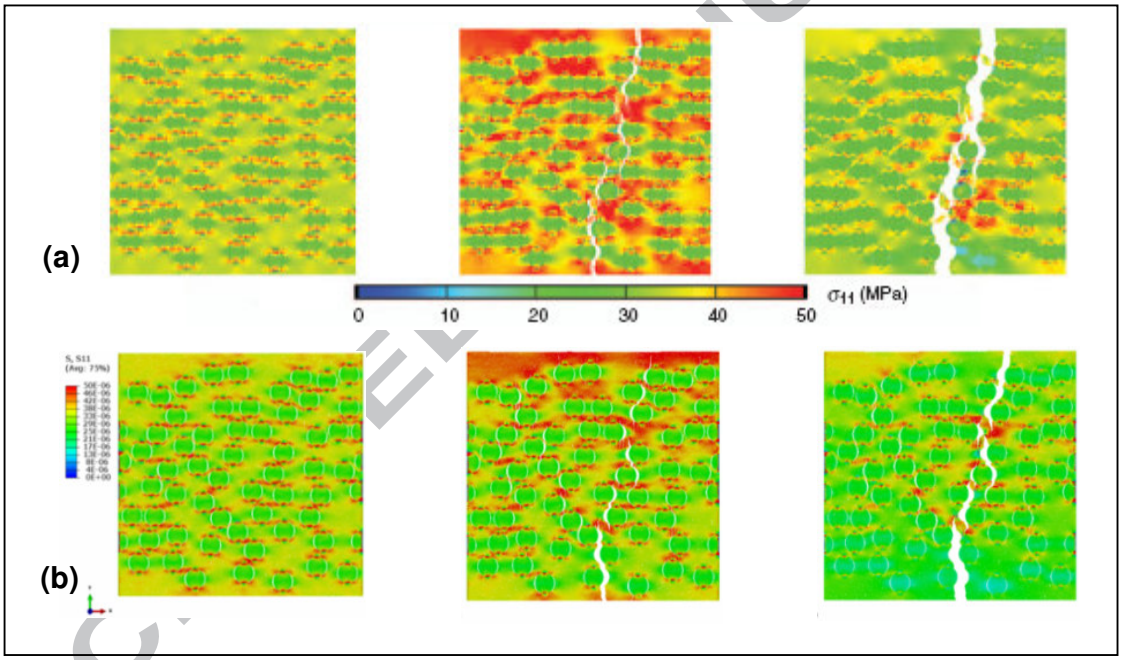

Figure 14: Comparison of stress contour plots on window size 125 µm and fibre volume fraction 30% at three different load steps: (a) results in (Cid Alfaro et al., 2010), (b) the present study.

To further demonstrate the importance of the interface material strength, a MeE of size 50µm^2 was simulated using the four interfacial types in Table 1. Figure 15 shows that the interface properties can greatly influence the meso- cracking mechanism which has important crack propagation effects on the macro-scale fracture. This is because local stress concentrations may potentially divert crack propagation for certain global boundary conditions. Experiments are thus necessary to examine the interface properties between fibres and the matrix and their mechanical effects.

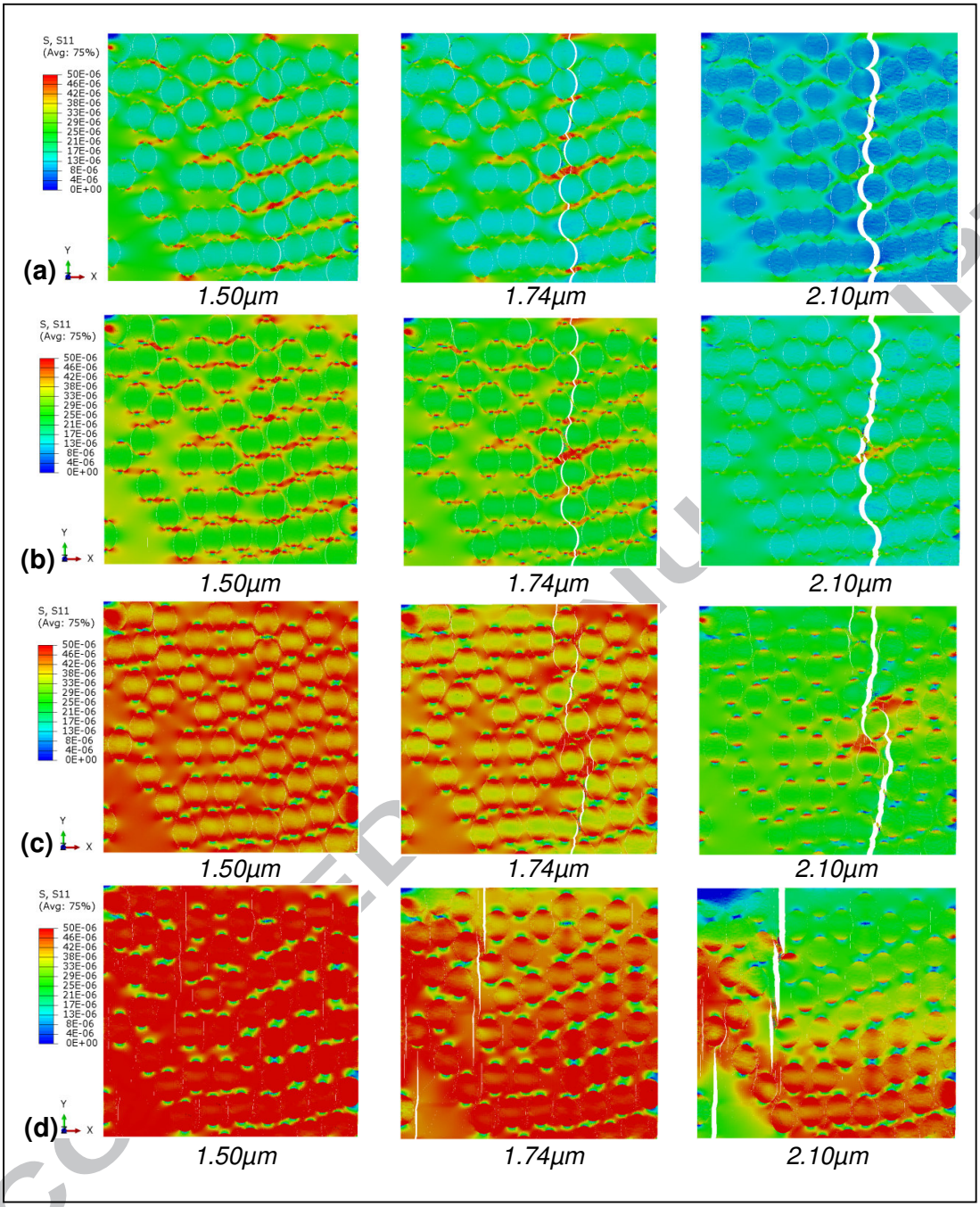

Figure 15: Stress contours at three load steps from MeE number 3 of size 50μm^2 using (a) poor, (b) weak, (c) strong and (d) perfect interface properties.

Boundary effects also influence crack initiation and propagation and therefore the overall dissipated energy. Figure 16 shows a two-crack dominant failure in the MeE size 100μm^2 image-based model using the G2-X type boundary conditions from Figure 2. In general, such effects were not observed on the other boundary types; thus only B1 type that is identical to G1 boundaries was further used in the scale coupling.

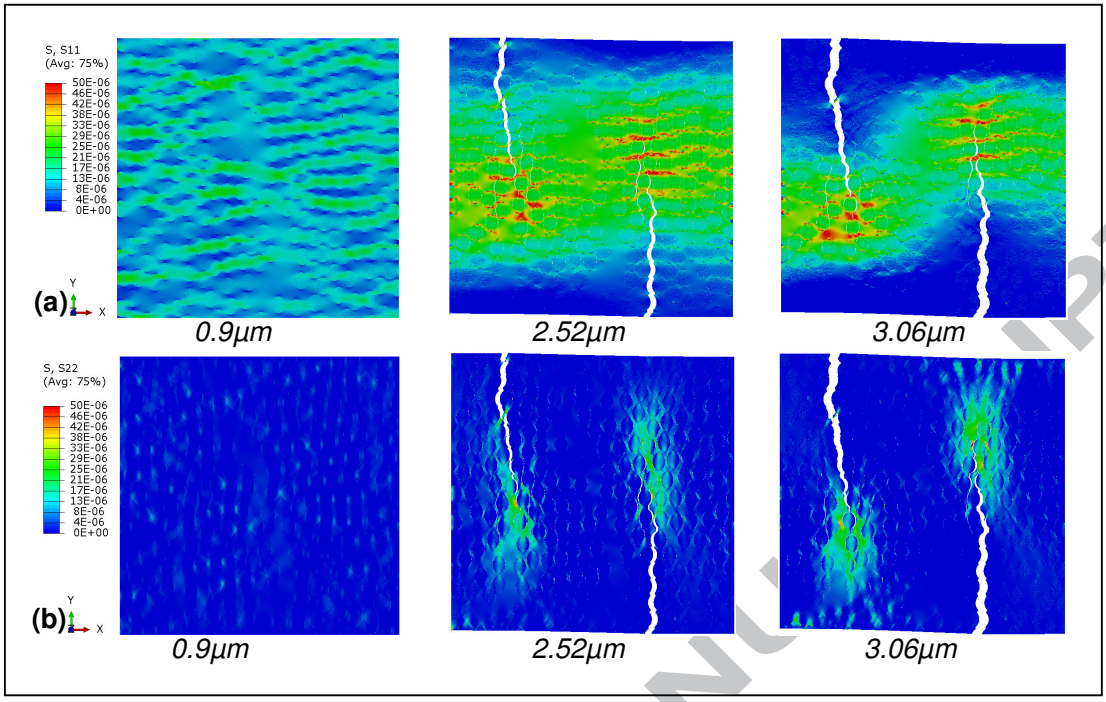

Figure 16: Stress contours at three loading steps using G2-X boundaries and weak interfacial properties showing a two dominant cracks failure in MeE size 100μm^2.

3.5. MeE size effects

Simulations for different MeE sizes, in increments of $10\mu m^2$ up to $100\mu m^2$, with centre at position 2 in Figure 11, were carried out to investigate size effects on crack paths and load-displacement curves. To avoid problems of localisation and mesh interface disclosure for zoom-out resolution, surface partitions were conducted so that the same mesh in smaller MeE is contained in larger ones (see Figure 17).

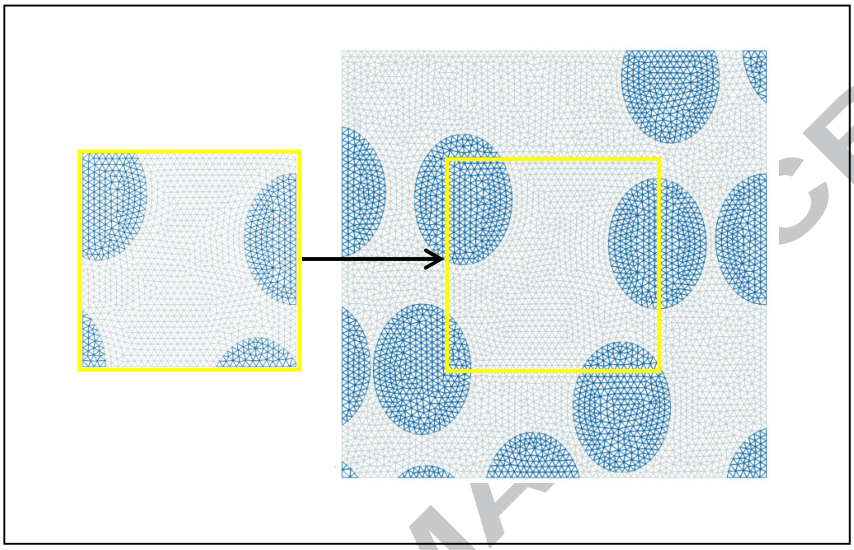

Figure 17: Image-based MeEs of size $10\mu m^2$ and $20\mu m^2$ illustrating the concept of partitioned concentric windows by preserving mesh topology.

The boundary conditions are given in Table 2. It is interesting to see that from one size to another, dissimilar crack paths appear when using G1-X loading conditions (see Figure 18 and Figure 19). This is expected since image based models have random inclusions and defects. Also the window sizes are often not sufficiently large to achieve a more uniform failure mode. A typical set of stress-displacement curves and the equivalent stress-strain curves are shown in Figure 20(a) & (b) respectively.

Figure 20(b) shows that a more sudden failure occurs as the MeE size increases. A strong size effect of the peak stress was found especially when weak interface properties were simulated. For all types of interfaces, the size effect of the strength decreases when the window size is larger than 20 - 30µm which was set as a minimum size of the MeE required for the scale transfer (see Figure 21). This is consistent with the statistical analysis of volume fractions in Figure 13.

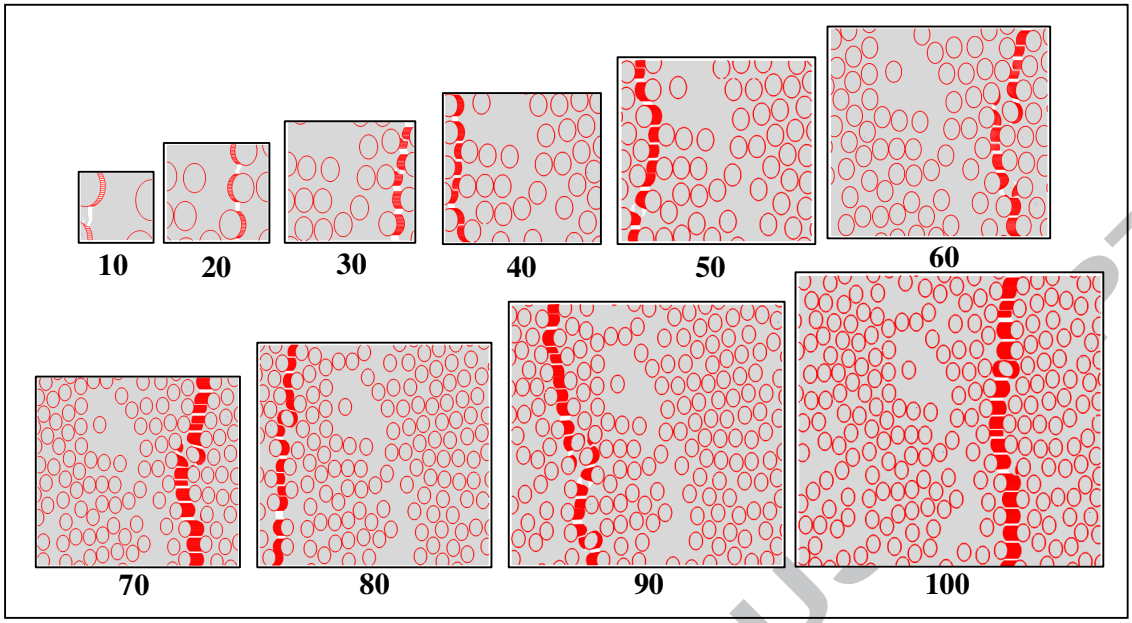

Figure 18: G1-X crack paths in different MeE sizes in μm for weak interface properties (the interface cohesive layer illustrated in red).

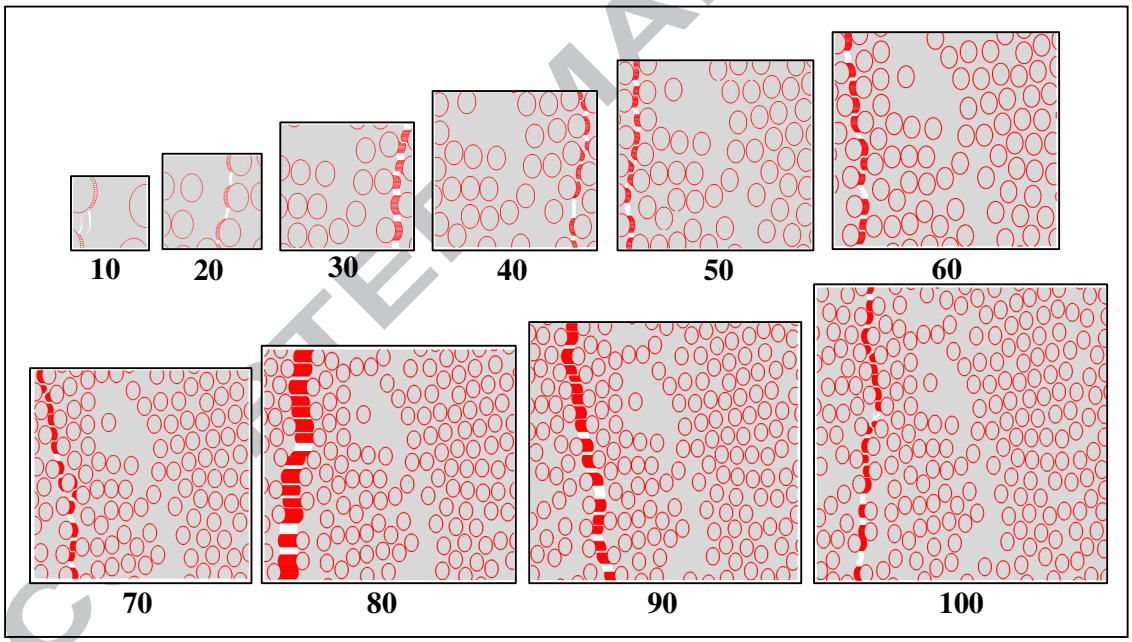

Figure 19: G1-X crack paths in different MeE sizes μm for strong interface properties (the interface cohesive layer illustrated in red).

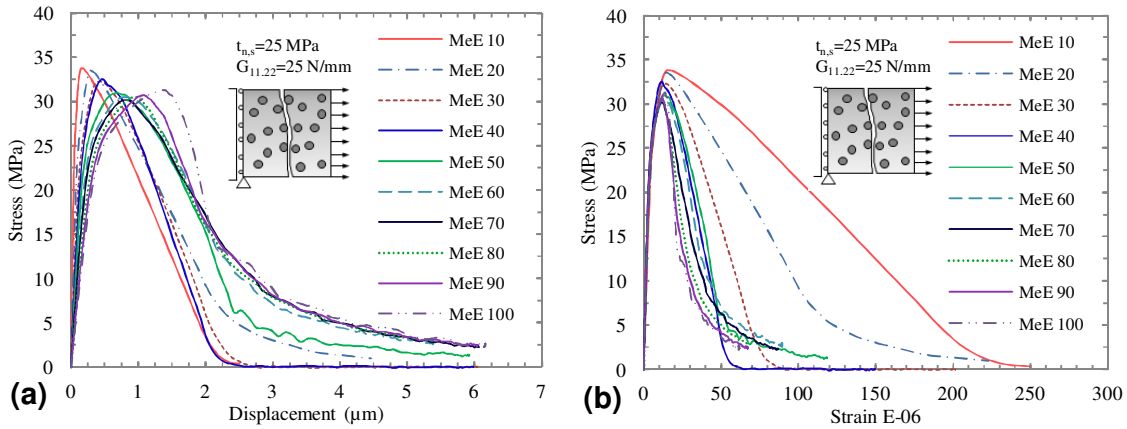

Figure 20: Stress-displacement and stress-strain curves for G2-X boundary conditions on MeE step $10\mu m^2$ to $100\mu m^2$ by using weak interface properties.

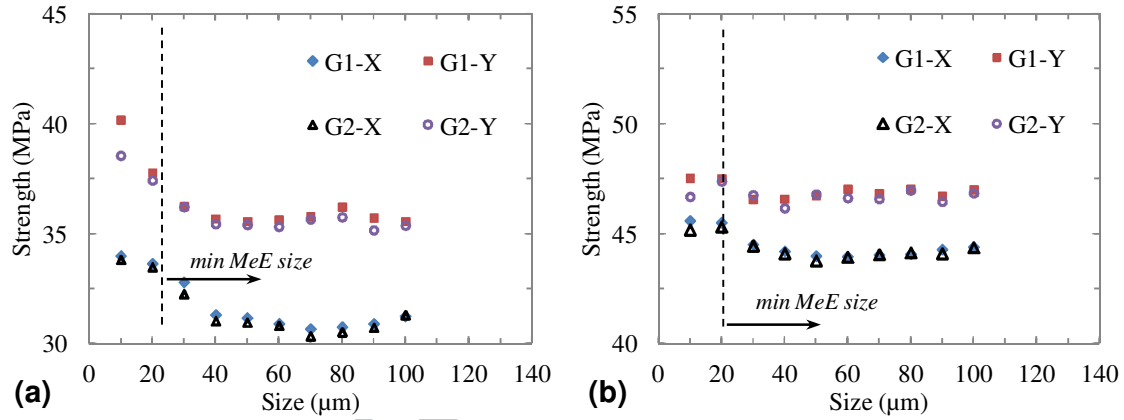

Figure 21: Size-strength results for MeE step $10\mu m^2$ to $100\mu m^2$ using (a) weak and (b) strong interface properties.

3.6. Stochastic MeE simulations

To investigate the effects of crack path bias and local orientation diversions in scale transfer, non-overlapping meso scale windows such as shown in Figure 3(a) were used in simulations first. The square MeE windows were simulated using the full set of boundary conditions in Table 2. The adaptive short to long-overlapping MeE grid discretisation was then used to tackle the problem of neighbouring crack paths bias. The idea is to share an overlapped support as to solve deformation compatibility. The concept may be also understood as an inverted overlapping limit. The upper bound corresponds to 2x computation of the same core MeE windows. This means that for long overlapping the integration must be limited by the distance between two neighbouring mass centres to avoid complicated double overlapping areas. This is useful particularly when strength and fracture energy variances are relatively small which holds in most composites with random distribution of features. Obviously, the short or narrow overlapping criteria will bring further computation savings as the computational areas are closer to the non-overlapping model. However, for both cases the main advantage is that the simulation of global large models can be parallelized to achieve high computational efficiency.

In Figure 22, the results for two main scenarios are presented as follows: (a,b,c) show weak interface crack paths and (d,e,f) show strong interface crack paths which were obtained using B1 boundaries on the orthotropic directions X and Y. Thus, given the random distribution of fibres, the interface layer between the fibres and matrix can be considered an intrinsic defect entity in this study. It can be seen that, when the non-overlapping method was used (a,d), the fracture paths rarely matched between the neighbouring MeE elements. When overlapping MeE windows were used, the matching rates were better in the case of weak interface properties (see Figure 22). In addition, there was a clear enhancement in crack site prediction compared with the non-overlapping results for cracks near edges (see and compare Figure 22 (a,b,c) & (d,e,f)). Figure 23 shows the variation of the predicted ultimate strengths with varying overlapping areas for different MeEs. Smaller strength variance with larger prediction errors were obtained for the strong interface models (see Figure 23 (b) MeE 12 & MeE 14).

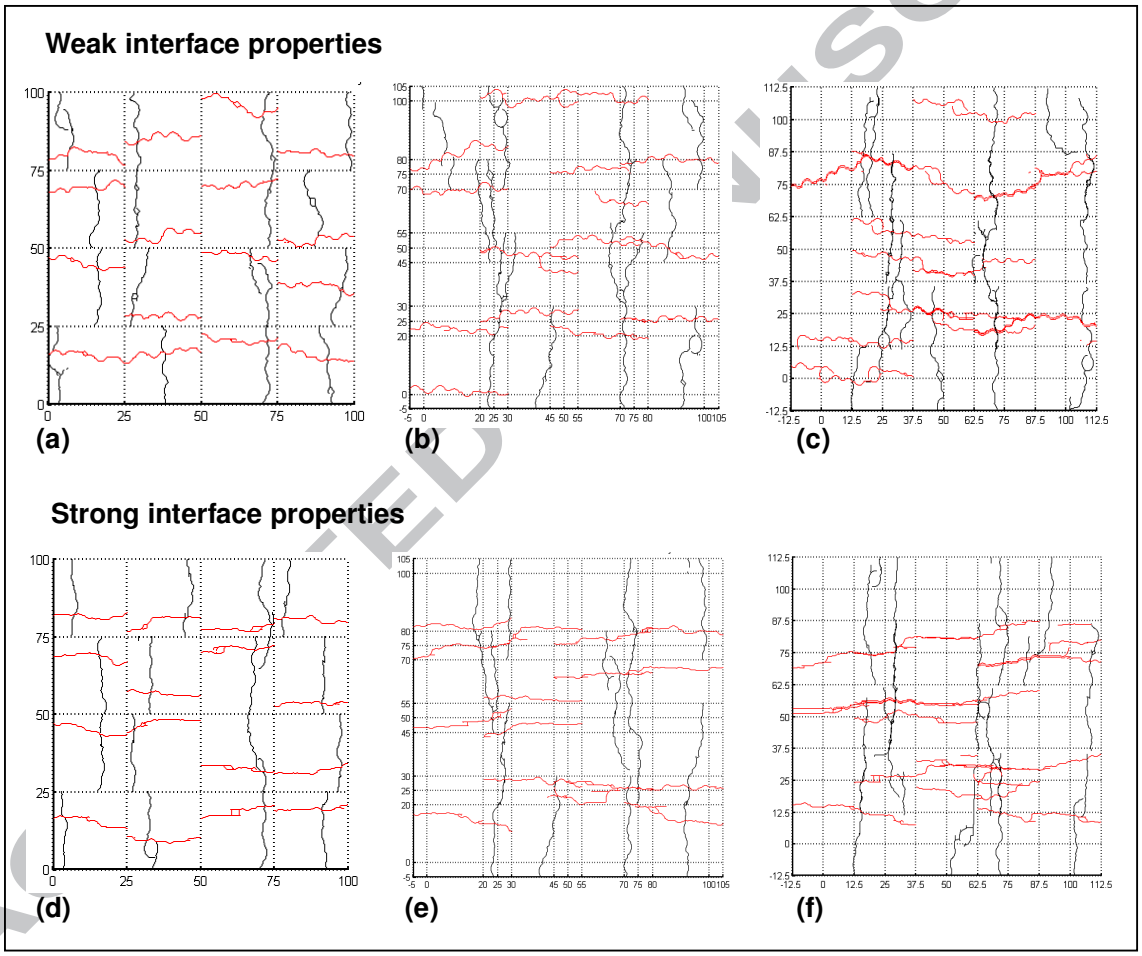

Figure 22: Crack paths for the adaptive size increasing non-overlapping MeE 16x25 (a,d) to short overlapping MeE16x35 (b,e) and long overlapping MeE16x50 (e,f). The two sets are from using weak interface properties (a,b,c) and strong interface properties (d,e,f).

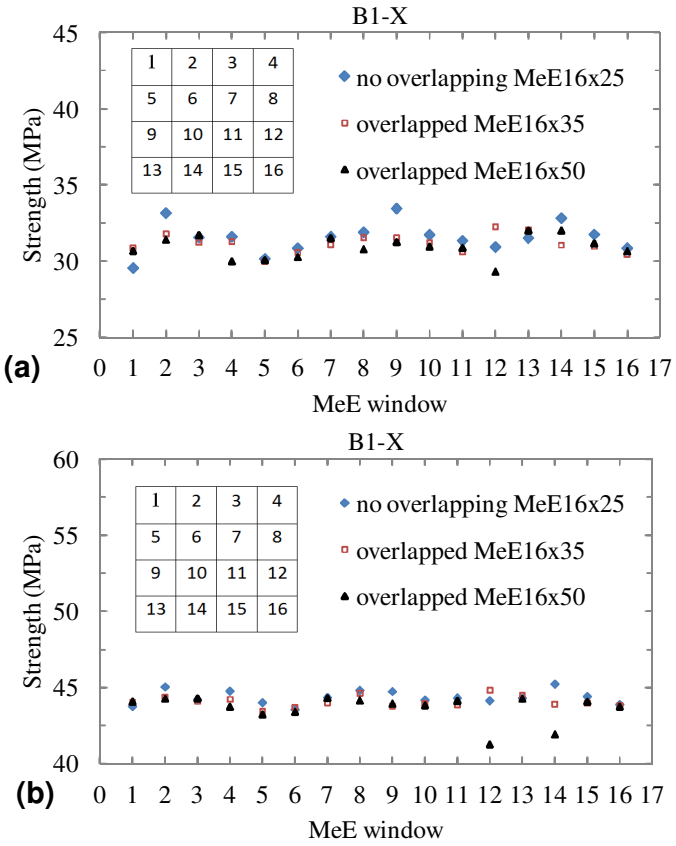

Figure 23: Variation of MeE strengths with different overlapping areas: (a) weak and (b) strong interface properties.

It should also be mentioned that for the scale transfer the B2-X and B2-Y boundary conditions in Figure 2 are necessary. The confidence domain for the softening part in such a case was limited to small sliding. This domain is equal to about 0.2µm which is approximately the size of one finite element used in the MeE simulations. A mesh example is shown in Figure 17.

In the following, the validation of the proposed multi-scale modelling method is established by comparing the detailed crack propagation results and energy dissipation mechanisms on both scales.

3.7. Comparison of meso and macro-crack propagation

This section elucidates the most convenient averaging approach to solving the scale transfer problem. The effective stiffness for each individual MeE was evaluated based on the results in Section 3.6. ABAQUS offers an orthotropic elasticity model which can be defined by a stiffness matrix. This matrix incorporates the effects of individual fracture modes on X and Y directions and the analytically combined effect of both (Simulia/Abaqus). A local coordinates system was also defined for the orthonormal directions X and Y.

Figure 24 & Figure 25 compare all the crack paths of uncoupled overlapping MeEs using B1 boundaries (shown in coloured lines) against the corresponding fully detailed MeE100 simulations (shown in black lines) using G1 and G2 cases on X and Y respectively.

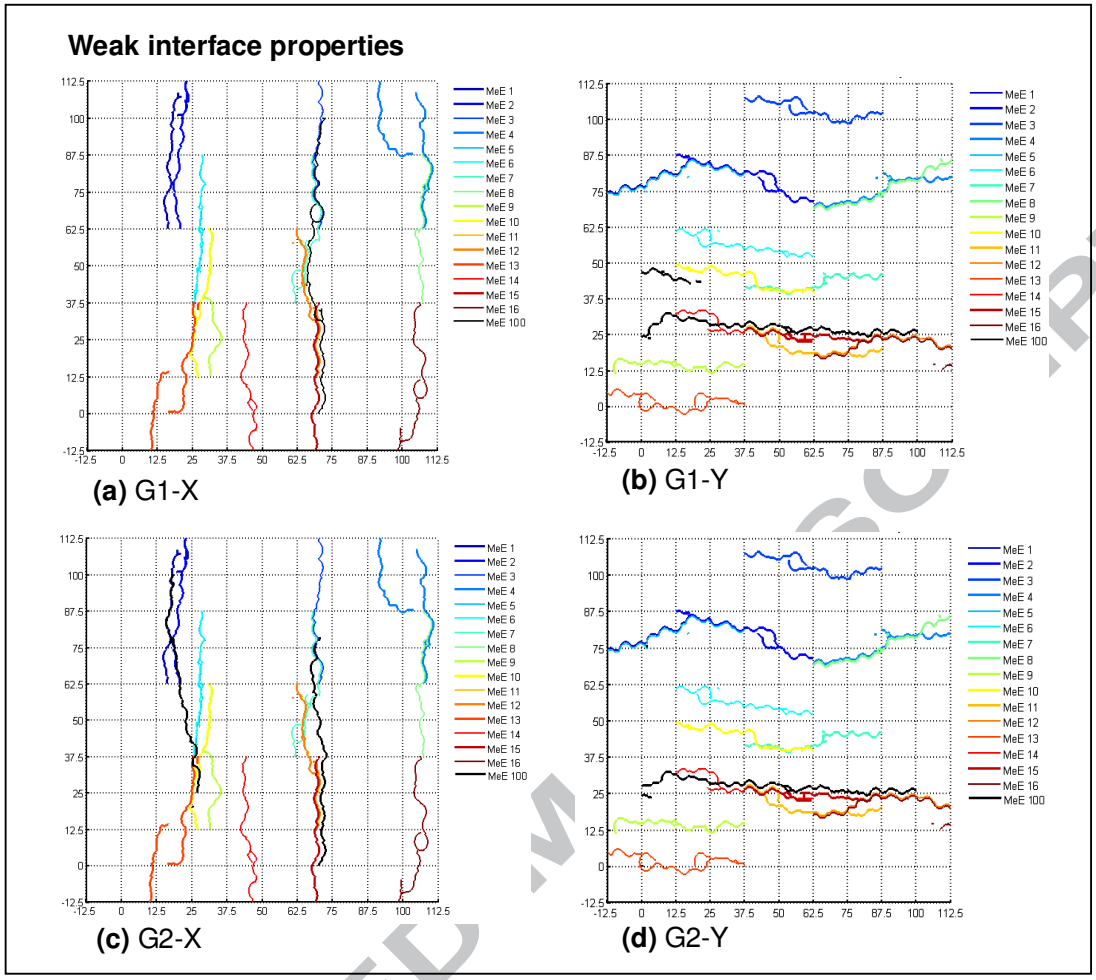

Figure 24: Comparison of separate crack paths between overlapping series MeE16x50 (shown in coloured lines) using B1 boundaries against full size MeE100 (shown in black lines): (a) G1-X; (b) G1-Y; (c) G2-X and (d) G2-Y for weak interface properties.

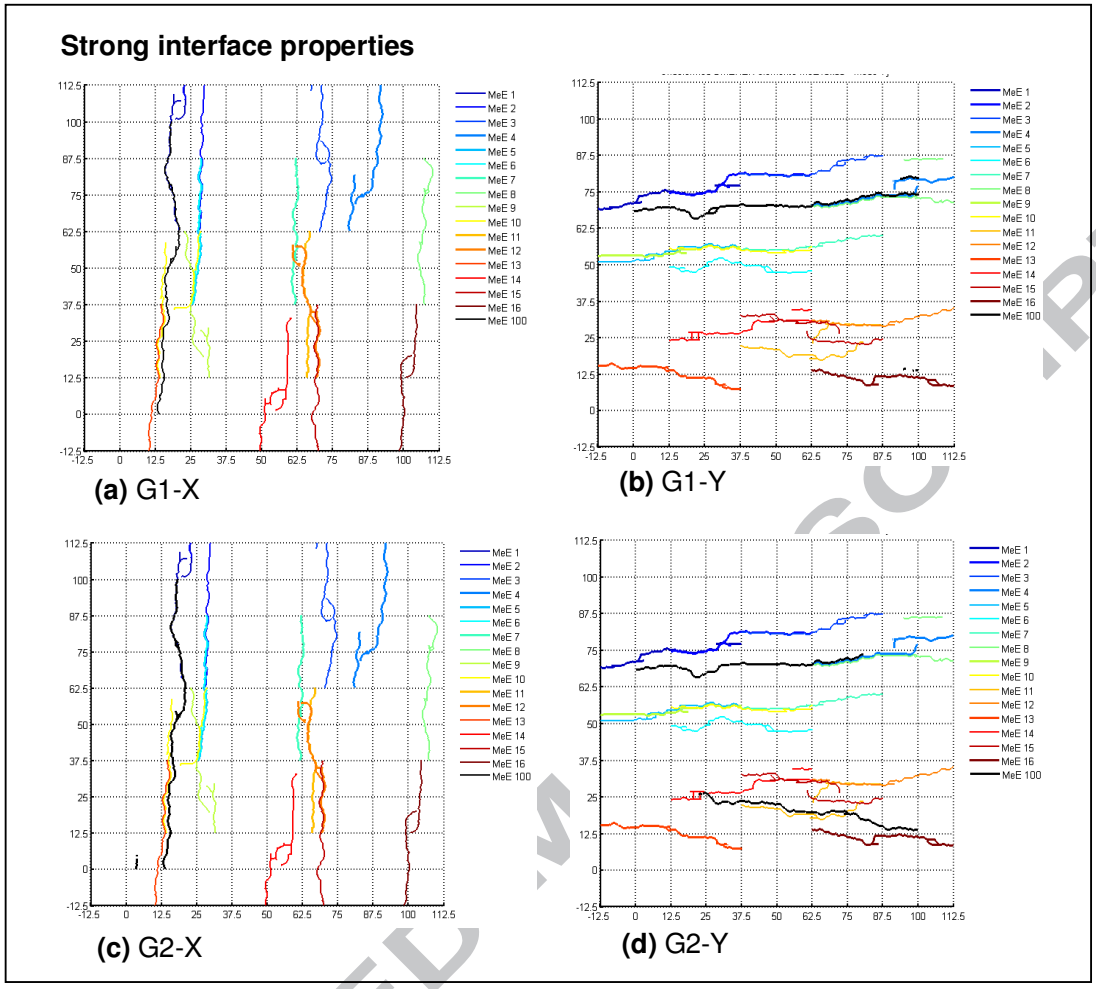

Figure 25: Comparison of separate crack paths between overlapping series MeE16x50 (shown in coloured lines) using B1 boundaries against full size MeE100 (shown in black lines): (a) G1-X; (b) G1-Y; (c) G2-X and (d) G2-Y for strong interface properties.

Figure 26 & Figure 27 compare the stress-displacement relationships of multi-scale models using overlapping series MeE16x50 and detailed MeE100 for weak and strong interface properties respectively. These models use reduced meshes and integrate material properties according to the methodology in Sections 2.3 & 2.4. The corresponding crack paths of both meso- and macro-simulations are also shown. It can be seen that the agreement was good when a single dominant crack path was modelled. If there are two distant crack paths, the matching locations could be established only in the case of weak interface properties (see the G2-X results in Figure 26 & Figure 27).

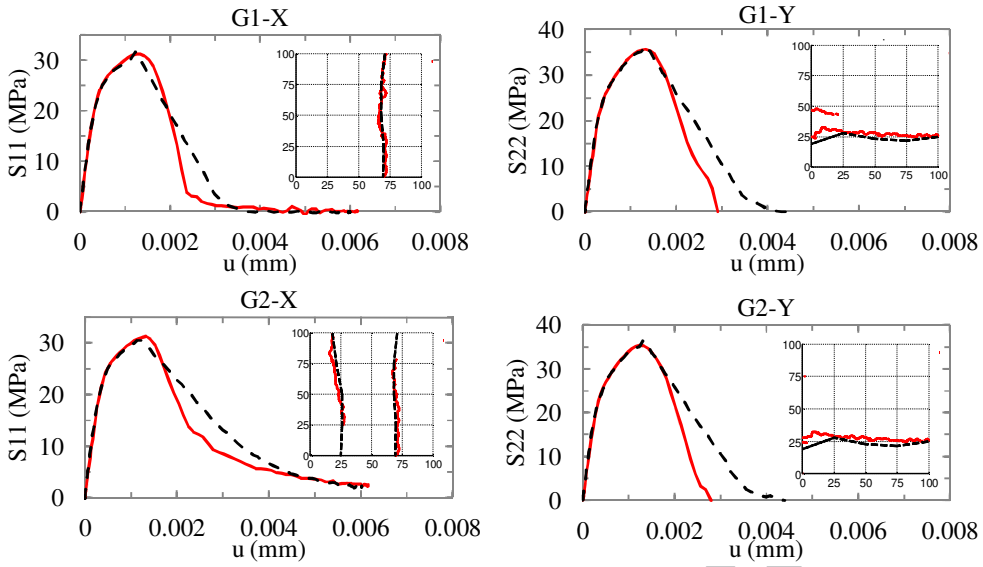

Figure 26: Nonlinear multi-scale results for weak interface properties using the overlapping concept vs fully detailed simulations (solid curve: detailed MeE100, dashed curve: using MeE 16x50 assembly).

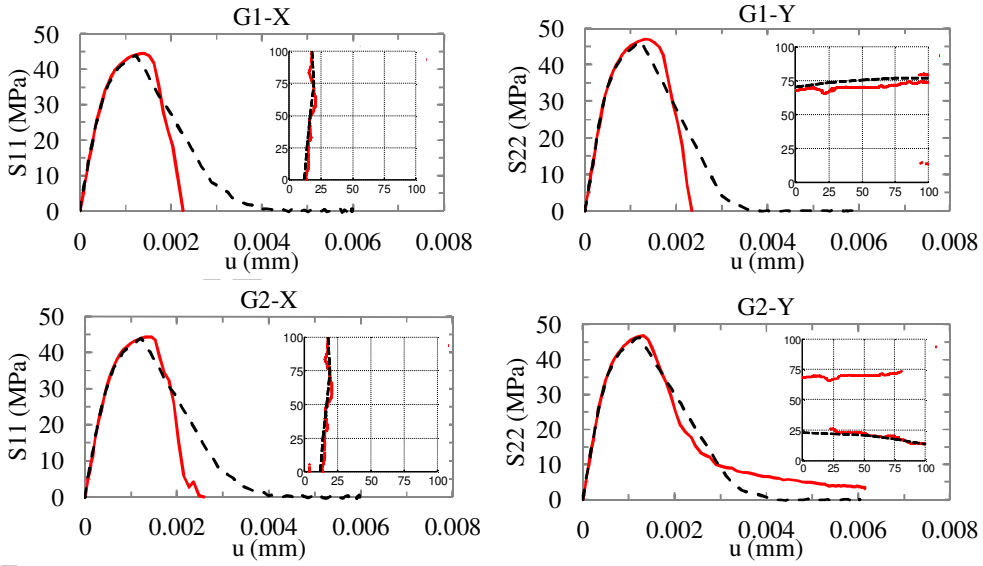

Figure 27: Nonlinear multi-scale results for strong interface properties using the overlapping concept vs fully detailed simulations (solid curve: detailed MeE100; dashed curve: using MeE16x50 assembly).

3.8. Application of the Bayesian inference

The Bayesian inference model in section 2.2 is then used to filter the non-matching crack paths in Fig. 24 and Fig. 25. The results are presented in Figure 28 & Figure 29, which show that highly nonlinear situations at global scale could be captured effectively by inserting macro-CIEs only where

necessary. The results are much improved with a good agreement especially for the two dominant crack paths situation in Figure 28 and Figure 29 using G2-X and G2-Y boundaries respectively.

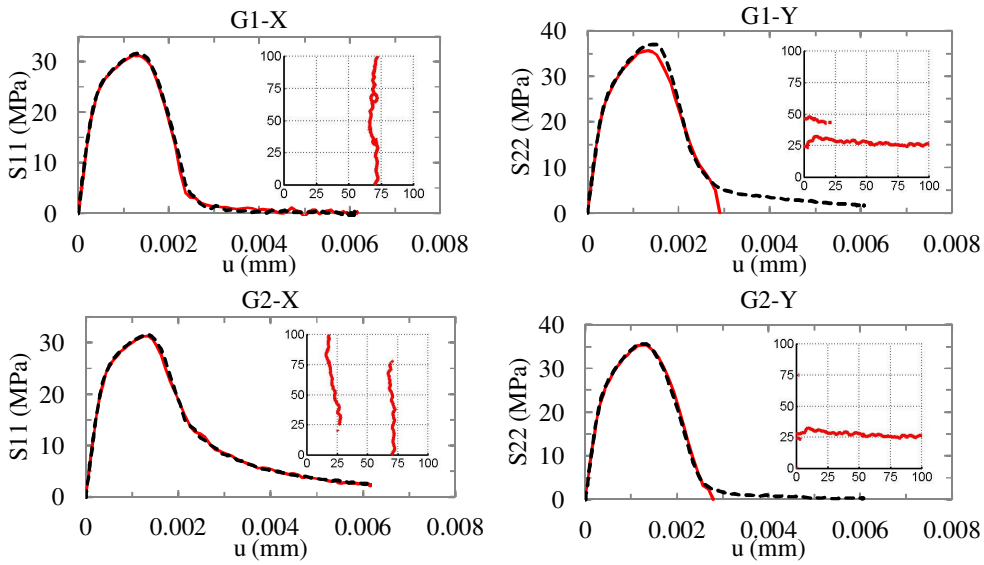

Figure 28: Comparison of simulation results using the multi-scale stochastic coupling strategy for weak interface properties. The solid curves represent the detailed geometry models (i.e. MeE size 100μm^2) and dashed curves are the Bayesian multi-scale models.

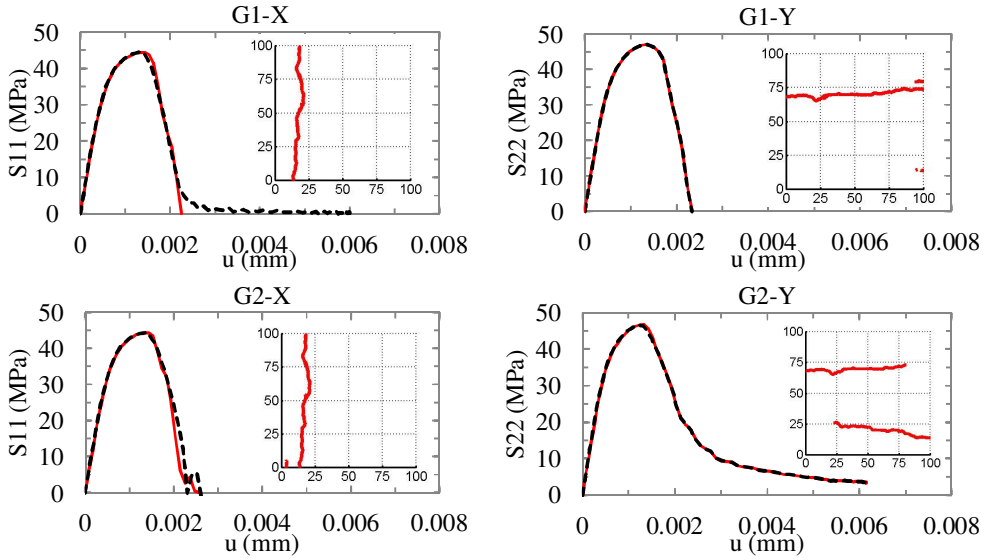

Figure 29: Comparison of simulation results using the multi-scale stochastic coupling strategy for strong interface properties. The solid curves represent the detailed geometry models (i.e. MeE size 100μm^2) and the dashed curves are the Bayesian multi-scale models.

4. CONCLUSIONS

This study has presented the development and validation, through a numerical case study, of a new multi-scale stochastic fracture mechanics framework (MsSFrM) for modelling cohesive fracture in heterogeneous materials. The following conclusions may be drawn:

(1) The selection of the meso-scale window sizes is highly related to the distribution of volume fractions. For accurate multi-scale couplings, the morphological continuity should be ensured by accurate mapping of the individual MeEs.

(2) Increasing the MeE size does not necessarily stabilise the fracture behaviour, thus invalidating the classical RVE approach. However, by choosing the appropriate MeE window size and resolving the boundary deformation compatibility via the overlapped windows concept, the crack bias effects can be minimized and therefore the scale transfer could be captured effectively.

(3) Energy mapping rules have been proposed for solving the scale coupling problem for different interface properties when the crack matching criteria is met. For defective materials, the short to long overlapping method may be used. For less defective materials, non-overlapping as for elastic studies or short overlapping can be used.

(4) The Bayesian inference model can be used to reduce the uncertainty of bias crack paths in the multi-scale transfer owing to its ability to update the state of belief using element cluster searches.

(5) The new multi-scale stochastic modelling method offers a more accurate modelling framework for multiphasic heterogeneous materials with various levels of defects. Heterogeneity features such as material defects, inclusions and voids can be incorporated at both scales.

(6) It should be noted that in the present method, all the MeEs are modelled independently under the same set of tensile and shear boundary conditions. This is not strictly valid even for the case studies under uniaxial tension in this paper. The results in terms of both final crack paths and load-displacement curves, however, are very good, probably due to the use of adaptively-increasing overlapping grids which may have ensured the deformation compatibility between adjacent MeEs to some extent. Research is much needed to integrate accurate algorithms for solving compatible boundary conditions of individual MeEs, such as those discussed by Oden et al (1999), so that the developed method can be applied to general situations.

Acknowledgements

This study is funded by a US Air Force EOARD grant (No. FA8655-12-1-2100) and an EPSRC grant (No. EP/J019763/1). We would like to thank Prof Costas Soutis at the Northwest Composite Centre in Manchester for providing CFRP materials, Dr William Bodel at Nuclear Graduate Research Group (NGRG) and C-Net for helping with acquisition of images and in-situ microscopy.

References

Aarnes, J. E., Krogstad, S. & Lie, K.-A. (2006) A Hierarchical Multiscale Method for Two-Phase Flow Based upon Mixed Finite Elements and Nonuniform Coarse Grids. *Multiscale Modeling & Simulation,* 5(2)**,** 337-363.

Belytschko, T. (2007) Research directions in computational and composite mechanics. *A Report of the United States National Committee on Theoretical and Applied Mechanics*.

Belytschko, T., Loehnert, S. & Song, J.-H. (2008) Multiscale aggregating discontinuities: A method for circumventing loss of material stability. *International Journal for Numerical Methods in Engineering,* 73(6)**,** 869-894.

Bosco, E., Kouznetsova, V. G. & Geers, M. G. D. (2015) Multi-scale computational homogenization-localization for propagating discontinuities using X-FEM. *International Journal for Numerical Methods in Engineering,* 102(3-4)**,** 496-527.

Caballero, A., Willam, K. J. & Carol, I. (2008) Consistent tangent formulation for 3D interface modeling of cracking/fracture in quasi-brittle materials. *Computer Methods in Applied Mechanics and Engineering,* 197(33-40)**,** 2804-2822.

Calo, V. M., Efendiev, Y., Galvis, J. & Ghommem, M. (2014) Multiscale empirical interpolation for solving nonlinear PDEs. *Journal of Computational Physics,* 278**,** 204-220.

Canal, L. P., González, C., Segurado, J. & Llorca, J. (2012) Intraply fracture of fiber-reinforced composites: Microscopic mechanisms and modeling. *Composites Science and Technology,* 72(11)**,** 1223-1232.

Carpinteri, A. & Chiaia, B. (1997) Multifractal Scaling Laws in the Breaking Disordered Materials.

Carpinteri, A., Chiaia, B. & Cornetti, P. (2002) A scale-invariant cohesive crack model for quasi-brittle materials. *Engineering Fracture Mechanics,* 69(2)**,** 207-217.

Chen, Y., Durlofsky, L. J., Gerritsen, M. & Wen, X. H. (2003) A coupled local–global upscaling approach for simulating flow in highly heterogeneous formations. *Advances in Water Resources,* 26(10)**,** 1041-1060.

Chung, E. T., Efendiev, Y. & Fu, S. (2014) Generalized Multiscale Finite Element Method for Elasticity Equations. *ArXiv e-prints,* (1408.5929).

Cid Alfaro, M. V., Suiker, A. S. J. & de Borst, R. (2010) Transverse Failure Behavior of Fibre-epoxy Systems. *Journal of Composite Materials*.

Coenen, E. W. C., Kouznetsova, V. G., Bosco, E. & Geers, M. G. D. (2012) A multi-scale approach to bridge microscale damage and macroscale failure: a nested computational homogenization-localization framework. *International Journal of Fracture,* 178(1-2)**,** 157-178.

Cusatis, G. & Cedolin, L. (2007) Two-scale study of concrete fracturing behavior. *Engineering Fracture Mechanics,* 74(1-2)**,** 3-17.

de Borst, R. (2008) Challenges in computational materials science: Multiple scales, multi-physics and evolving discontinuities. *Computational Materials Science,* 43(1)**,** 1-15.

Desmorat, R. & Lemaitre, J. (2001) A Two-Scale Model for Quasi-Brittle and Fatigue Damage. *In:* Jean, L. (ed.) *Handbook of Materials Behavior Models.* Burlington: Academic Press.

Dirrenberger, J., Forest, S. & Jeulin, D. (2014) Towards gigantic RVE sizes for 3D stochastic fibrous networks. *International Journal of Solids and Structures,* 51(2)**,** 359-376.

Efendiev, Y., Galvis, J., Li, G. & Presho, M. (2014) Generalized multiscale finite element methods: Oversampling strategies. 12(6)**,** 465-484.

Efendiev, Y., Hou, T. Y. & Ginting, V. (2004) Multiscale Finite Element Methods for Nonlinear Problems and Their Applications. 553-589.

Fish, J. (2011) Multiscale Modeling and Simulation of Composite Materials and Structures

Multiscale Methods in Computational Mechanics. *In:* de Borst, R. & Ramm, E. (eds.). Springer Berlin / Heidelberg.

Fish, J. & Shek, K. (1999) Finite deformation plasticity for composite structures: Computational models and adaptive strategies. *Computer Methods in Applied Mechanics and Engineering,* 172(1–4)**,** 145-174.

Gao, K., Fu, S., Gibson Jr, R. L., Chung, E. T. & Efendiev, Y. (2014) Generalized Multiscale Finite-Element Method (GMsFEM) for elastic wave propagation in heterogeneous, anisotropic media.

Ghosh, S., Bai, J. & Raghavan, P. (2007) Concurrent multi-level model for damage evolution in microstructurally debonding composites. *Mechanics of Materials,* 39(3)**,** 241-266.

Ghosh, S. & Paquet, D. (2013) Adaptive concurrent multi-level model for multi-scale analysis of ductile fracture in heterogeneous aluminum alloys. *Mechanics of Materials,* 65(0)**,** 12-34.

Gitman, I. M., Askes, H. & Sluys, L. J. (2007) Representative volume: Existence and size determination. *Engineering Fracture Mechanics,* 74(16)**,** 2518-2534.

Gitman, I. M., Askes, H. & Sluys, L. J. (2008) Coupled-volume multi-scale modelling of quasi-brittle material. *European Journal of Mechanics - A/Solids,* 27(3)**,** 302-327.

González, C. & Llorca, J. (2006) Multiscale modeling of fracture in fiber-reinforced composites. *Acta Materialia,* 54(16)**,** 4171-4181.

González, C. & Llorca, J. (2007) Mechanical behavior of unidirectional fiber-reinforced polymers under transverse compression: Microscopic mechanisms and modeling. *Composites Science and Technology,* 67(13)**,** 2795-2806.

Graham, S. & Yang, N. (2002) Representative volumes of materials based on microstructural statistics.

Greco, F., Leonetti, L. & Lonetti, P. (2013) A two-scale failure analysis of composite materials in presence of fiber/matrix crack initiation and propagation. *Composite Structures,* 95(0)**,** 582-597.

Hashin, Z. (1965) On elastic behaviour of fibre reinforced materials of arbitrary transverse phase geometry. *Journal of the Mechanics and Physics of Solids,* 13(3)**,** 119-134.

Hautefeuille, M., Colliat, J. B., Ibrahimbegovic, A., Matthies, H. G. & Villon, P. (2012) A multi-scale approach to model localized failure with softening. *Computers & Structures,* 94-95**,** 83-95.

Hill, R. (1963) Elastic properties of reinforced solids: Some theoretical principles. *Journal of the Mechanics and Physics of Solids,* 11(5)**,** 357-372.

Hillerborg, A., Modéer, M. & Petersson, P. E. (1976) Analysis of crack formation and crack growth in concrete by means of fracture mechanics and finite elements. *Cement and Concrete Research,* 6(6)**,** 773-781.

Hou, T. Y. & Wu, X.-H. (1997) A Multiscale Finite Element Method for Elliptic Problems in Composite Materials and Porous Media. *Journal of Computational Physics,* 134(1)**,** 169-189.

Huang, Y., Yang, Z., Ren, W., Liu, G. & Zhang, C. (2015) 3D meso-scale fracture modelling and validation of concrete based on in-situ X-ray Computed Tomography images using damage plasticity model. *International Journal of Solids and Structures,* 67–68**,** 340-352.

Kaczmarczyk, Ł., Pearce, C. J., Bićanić, N. & de Souza Neto, E. (2010) Numerical multiscale solution strategy for fracturing heterogeneous materials. *Computer Methods in Applied Mechanics and Engineering,* 199(17–20)**,** 1100-1113.

Kanouté, P., Boso, D., Chaboche, J. & Schrefler, B. (2009) Multiscale Methods for Composites: A Review. *Archives of Computational Methods in Engineering,* 16(1)**,** 31-75.

Kassner, M. E., Nemat-Nasser, S., Suo, Z., Bao, G., Barbour, J. C., Brinson, L. C., Espinosa, H., Gao, H., Granick, S., Gumbsch, P., Kim, K.-S., Knauss, W., Kubin, L., Langer, J., Larson, B. C., Mahadevan, L., Majumdar, A., Torquato, S. & van Swol, F. (2005) New directions in mechanics. *Mechanics of Materials,* 37(2–3)**,** 231-259.

Li, Y., McDowell, D. L. & Zhou, M. (2013) Computational prediction of fracture toughness of polycrystalline metals. *13th International Conference on Fracture, Beijing, China,* (June 16–21, 2013).

Loehnert, S. & Belytschko, T. (2007) A multiscale projection method for macro/microcrack simulations. *International Journal for Numerical Methods in Engineering,* 71(12)**,** 1466-1482.

López, C. M., Carol, I. & Aguado, A. (2007) Meso-structural study of concrete fracture using interface elements. II: compression, biaxial and Brazilian test. *Materials and Structures,* 41(3)**,** 601-620.

Markovic, D. & Ibrahimbegovic, A. (2004) On micro–macro interface conditions for micro scale based FEM for inelastic behavior of heterogeneous materials. *Computer Methods in Applied Mechanics and Engineering,* 193(48–51)**,** 5503-5523.

Miehe, C. & Bayreuther, C. G. (2007) On multiscale FE analyses of heterogeneous structures: from homogenization to multigrid solvers. *International Journal for Numerical Methods in Engineering,* 71(10)**,** 1135-1180.

Nguyen, V. P., Lloberas-Valls, O., Stroeven, M. & Sluys, L. J. (2012a) Computational homogenization for multiscale crack modeling. Implementational and computational aspects. *International Journal for Numerical Methods in Engineering,* 89(2)**,** 192-226.

Nguyen, V. P., Stroeven, M. & Sluys, L. J. (2011) Multiscale continuous and discontinuous modeling of heterogeneous materials: a review on recent developments. *Journal of Multiscale Modelling,* 03(04)**,** 229-270.

Nguyen, V. P., Stroeven, M. & Sluys, L. J. (2012b) An enhanced continuous–discontinuous multiscale method for modeling mode-I cohesive failure in random heterogeneous quasi-brittle materials. *Engineering Fracture Mechanics,* 79(0)**,** 78-102.

Oden, J. T., Belytschko, T., Babuska, I. & Hughes, T. J. R. (2003) Research directions in computational mechanics. *Computer Methods in Applied Mechanics and Engineering,* 192(7–8)**,** 913-922.

Oden, J. T., Vemaganti, K., Moës, N. (1999) Hierarchical modeling of heterogeneous solids. Computer Methods in Applied Mechanics and Engineering, 172(1–4), 3–25.

Park, K. & Paulino, G. H. (2012) Computational implementation of the PPR potential-based cohesive model in ABAQUS: Educational perspective. *Engineering Fracture Mechanics,* 93**,** 239-262.

Phu Nguyen, V., Lloberas-Valls, O., Stroeven, M. & Johannes Sluys, L. (2010) On the existence of representative volumes for softening quasi-brittle materials – A failure zone averaging scheme. *Computer Methods in Applied Mechanics and Engineering,* 199(45–48)**,** 3028-3038.

Ren, W., Yang, Z., Sharma, R., Zhang, C. & Withers, P. J. (2015) Two-dimensional X-ray CT image based meso-scale fracture modelling of concrete. *Engineering Fracture Mechanics,* 133**,** 24-39.

Ruiz, G., Pandolfi, A. & Ortiz, M. (2001) Three-dimensional cohesive modeling of dynamic mixed-mode fracture. *International Journal for Numerical Methods in Engineering,* 52(12)**,** 97-120.

Simulia/Abaqus. - Abaqus theory manual. Online version 6.12.

Su, X., Yang, Z. & Liu, G. (2010) Monte Carlo simulation of complex cohesive fracture in random heterogeneous quasi-brittle materials: a 3D study. *International Journal of Solids and Structures*, 47(17), 2336-2345.

Trias, D., Costa, J., Fiedler, B., Hobbiebrunken, T. & Hurtado, J. E. (2006a) A two-scale method for matrix cracking probability in fibre-reinforced composites based on a statistical representative volume element. *Composites Science and Technology,* 66(11–12)**,** 1766-1777.

Trias, D., Costa, J., Mayugo, J. A. & Hurtado, J. E. (2006b) Random models versus periodic models for fibre reinforced composites. *Computational Materials Science,* 38(2)**,** 316-324.

Trias, D., Costa, J., Turon, A. & Hurtado, J. E. (2006c) Determination of the critical size of a statistical representative volume element (SRVE) for carbon reinforced polymers. *Acta Materialia,* 54(13)**,** 3471-3484.

Vaughan, T. J. & McCarthy, C. T. (2011) Micromechanical modelling of the transverse damage behaviour in fibre reinforced composites. *Composites Science and Technology,* 71(3)**,** 388-396.

Wang, X. F., Yang, Z. J., Yates, J. R., Jivkov, A. P. & Zhang, C. (2015) Monte Carlo simulations of mesoscale fracture modelling of concrete with random aggregates and pores. *Construction and Building Materials,* 75**,** 35-45.

Xu, Q., Chen, J., Li, J. & Wang, M. (2013) Multi-scale numerical model for simulating concrete material based on fractal theory. *Acta Mechanica Solida Sinica,* 26(4)**,** 344-352.

Xu, X. F. & Chen, X. (2009) Stochastic homogenization of random elastic multi-phase composites and size quantification of representative volume element. *Mechanics of Materials,* 41(2)**,** 174-186.

Xu, X. F. & Graham-Brady, L. (2005) A stochastic computational method for evaluation of global and local behavior of random elastic media. *Computer Methods in Applied Mechanics and Engineering,* 194(42–44)**,** 4362-4385.

Yang, Z. J., Su, X. T., Chen, J. F. & Liu, G. H. (2009) Monte Carlo simulation of complex cohesive fracture in random heterogeneous quasi-brittle materials. *International Journal of Solids and Structures,* 46(17)**,** 3222-3234.

Yu, R. C., Zhang, X. & Ruiz, G. (2008) Cohesive modeling of dynamic fracture in reinforced concrete. *Computers and Concrete,* Volume 5, Issue 4, 2008, pp.389-400.

NOMENCLATURE

Acronyms:

MsSFrM	-multiscale stochastic fracture mechanics.
MeE	-meso-scale element.
MaE	-macro-scale element.
CIE	-cohesive interface element.
BCs	-boundary conditions.
MSA	-merging and splitting approach.
CDA	-crack path decomposition approach.

Boundary conditions:

B1-X, B2-X	-meso-scale boundary conditions on X direction.
B1-Y, B2-Y	-meso-scale boundary conditions on Y direction.
G1-X, G2-X	-global-scale boundary conditions used for validation on X direction.
G1-Y, G2-Y	-global-scale boundary conditions used for validation on Y direction.

Algebra:

C	-kernel crack path.

H_k	-hidden key-points rendered on the stochastic crack path C.
$P(C)$	-probability of crack path C evaluated as a surface/path integral.
$P(E\|C)$	-prior probability of neighboring crack E to match the kernel crack path C. This probability is evaluated as a surface/ path integral.
$P(C\|E)$	-Bayesian updated probability of crack C given an overlapped neighboring crack path E. This probability is evaluated using a Bayesian inference model.
C_m	-set of crack paths over a neighboring cluster.
L_i	-reduced order integration line fitted on a random crack path.
σ_f	-ultimate strength equivalent to the onset of fracture.
$\sigma_{f,u} = \sigma(u)$	-softening evolution based on the ultimate strength pitch.
G_f	-fracture energy
$G_{f,short}$	-fracture energy evaluated for short overlapping criteria.
$G_{f,long}$	-fracture energy evaluated for long overlapping criteria.
u	-finite displacement.
u_f	-final displacement.
d	-scalar degradation variable.

d_{short} -scalar degradation variable evaluated for short overlapping criteria.

d_{long} -scalar degradation variable evaluated for long overlapping criteria.

V_f -fibre volume fraction.

V_m -matrix volume fraction.